

AD \_\_\_\_\_

Award Number: DAMD17-00-1-0467

TITLE: The Molecular Basis of Double-Strand DNA Break Repair:  
Crystal Structure of the RAD52/RPA Complex

PRINCIPAL INVESTIGATOR: Doba D. Jackson  
Gloria Borgstahl, Ph.D.

CONTRACTING ORGANIZATION: The University of Toledo  
Toledo, Ohio 43606-3390

REPORT DATE: July 2002

TYPE OF REPORT: Annual Summary

PREPARED FOR: U.S. Army Medical Research and Materiel Command  
Fort Detrick, Maryland 21702-5012

DISTRIBUTION STATEMENT: Approved for Public Release;  
Distribution Unlimited

The views, opinions and/or findings contained in this report are those of the author(s) and should not be construed as an official Department of the Army position, policy or decision unless so designated by other documentation.

20030211 181

**REPORT DOCUMENTATION PAGE**Form Approved  
OMB No. 074-0188

Public reporting burden for this collection of information is estimated to average 1 hour per response, including the time for reviewing instructions, searching existing data sources, gathering and maintaining the data needed, and completing and reviewing this collection of information. Send comments regarding this burden estimate or any other aspect of this collection of information, including suggestions for reducing this burden to Washington Headquarters Services, Directorate for Information Operations and Reports, 1215 Jefferson Davis Highway, Suite 1204, Arlington, VA 22202-4302, and to the Office of Management and Budget, Paperwork Reduction Project (0704-0188), Washington, DC 20503

<b>1. AGENCY USE ONLY (Leave blank)</b>		<b>2. REPORT DATE</b> July 2002	<b>3. REPORT TYPE AND DATES COVERED</b> Annual Summary (15 Jul 00 -14 Jun 02)	
<b>4. TITLE AND SUBTITLE</b> The Molecular Basis of Double-Strand DNA Break Repair: Crystal Structure of the RAD52/RPA Complex			<b>5. FUNDING NUMBERS</b> DAMD17-00-1-0467	
<b>6. AUTHOR(S)</b> Doba D. Jackson Gloria Borgstahl, Ph.D.				
<b>7. PERFORMING ORGANIZATION NAME(S) AND ADDRESS(ES)</b> The University of Toledo Toledo, Ohio 43606-3390  <b>Email: <u>ddj10@psu.edu</u></b>			<b>8. PERFORMING ORGANIZATION REPORT NUMBER</b>	
<b>9. SPONSORING / MONITORING AGENCY NAME(S) AND ADDRESS(ES)</b> U.S. Army Medical Research and Materiel Command Fort Detrick, Maryland 21702-5012			<b>10. SPONSORING / MONITORING AGENCY REPORT NUMBER</b>	
<b>11. SUPPLEMENTARY NOTES</b>				
<b>12a. DISTRIBUTION / AVAILABILITY STATEMENT</b> Approved for Public Release; Distribution Unlimited			<b>12b. DISTRIBUTION CODE</b>	
<b>13. ABSTRACT (Maximum 200 Words)</b>  none provided				
<b>14. SUBJECT TERMS</b> DNA break repair, RAD52/RPA complex			<b>15. NUMBER OF PAGES</b> 35	
			<b>16. PRICE CODE</b>	
<b>17. SECURITY CLASSIFICATION OF REPORT</b> Unclassified	<b>18. SECURITY CLASSIFICATION OF THIS PAGE</b> Unclassified	<b>19. SECURITY CLASSIFICATION OF ABSTRACT</b> Unclassified	<b>20. LIMITATION OF ABSTRACT</b> Unlimited	

## Table of Contents

Cover.....	1
SF 298.....	2
Table of Contents.....	3
Introduction.....	4
Body.....	5
Key Research Accomplishments.....	7
Reportable Outcomes.....	8
Conclusions.....	8
Appendices.....	9

## Introduction

Human Rad52 and RPA are involved in the early steps of double-stranded break repair. The repair of double-stranded breaks in chromosomal DNA is of critical importance for the maintenance of genomic integrity. Rad52 and RPA interact in vivo and in vitro and its interaction is involved in the mechanism of double-strand break repair.

In this research, the objective was grouped into four parts:

- 1) To define the minimum interacting regions on Rad52 and RPA.
- 2) To identify equilibrium binding conditions that favor the formation of the complex.
- 3) To develop soluble and active fragments of Rad52 and RPA, each with the particular binding domains.
- 4) To grow x-ray quality crystals of the soluble active fragments preferably in the complexed form.
- 5) To solve the crystallographic phase problem and interpret a three dimensional map of the structure.
- 6) To publish any significant findings

The results obtained are listed here in this summary and mentioned briefly here. First we have defined two regions of RPA (one on RPA32 and one on RPA70) that interact with Rad52. We have also localized both of these RPA binding sites to an 85 amino acid region near the C-terminus of Rad52. Second we have determined ionic strength, pH and detergents that maximize the formation of the complex while minimizing the formation of aggregates and free subunits. Third we have developed, optimized the purification of soluble active fragments of rad52 and RPA (Rad52(218-418) and RPA 14/32). We have also published our significant findings and are shown here in the appendix. We regreably are not reporting the crystallization and structure of the Rad52/PA complex however, we have found a condition for Rad52(218-418) alone for crystallization. Crystals of RPA 14/32 were reported previously and were obtained in the Borgstahl laboratory. The PI has moved on to a PostDoc position in another laboratory and the the project fr solving the structure of the Rad52/RPA complex will be taken over by someone else in the future.



## **Research Summary**

### **Specific aim 1- Characterize the RPA and Rad52 binding regions.**

The region RPA binds Rad52 and Rad52 binding to RPA were fully defined during the first year of this report. The characterization of RPA/Rad52 binding sites were done using the modified ELISA protocol as previously described (last summary and described in appendix references #1 and #3). Also the DNA binding ability was also investigated by immunoprecipitated solution complexes (discussed in the original proposal) and gel mobility shift assays in collaboration with Dr Marc wold (sent letter of collaboration for this project and described in appendix references #3). The objective of this specific aim was also to publish the significant findings which was done (appendix reference #3).

#### **Characterization of the RPA & Rad52 binding surfaces**

Protein-protein interactions play an important role in Rad52-mediated double-strand break repair (1,2). This specific aim is set out to characterize the binding surfaces on both RPA and Rad52. A more complete description of the Rad52/RPA binding regions will be referred to the supplied appendix references #1 and #3. I will briefly summarize the results found.

- 1) Using a series of RPA deletion mutants, two binding sites on RPA for Rad52 were confirmed. A strong interaction on RPA32 requires residues from 241-271 on the C-terminus of RPA32 (referred to here now on as RPA32CTD). A weaker interaction on the central section of the RPA70 subunit localized between residues 168 and 326.
- 2) Binding sites for the RPA32 and RPA70 subunits on Rad52 was found to reside within residues 218-303 using a series of Rad52 deletion mutants. Each subunit of RPA has distinct determinants for binding specifically to that particular subunit as shown on a competition ELISA (see figure 1).
- 3) A putative binding surface on RPA70 was identified from residues 218-236 using sequence homology to the corresponding surface on RPA32. The putative binding site was found to be 32% identical and 79% similar to the RPA32 binding site.

### **Specific aim 2- Develop a soluble active complex that will mimic RPA, Rad52 interaction for the purpose of crystallization.**

The RPA/Rad52 binding studies have determined that two regions on RPA are in contact with Rad52 in the Rad52/RPA complex. In our original research proposal we proposed the RPA 14/32 heterodimer and Rad52 (218-418) complex for crystallization. RPA 14/32 heterodimer is a suitable mutant of RPA for crystallization and our laboratory we have previously established several crystal forms of the RPA 14/32 heterodimer. Here I will present the development of the C-terminal construct of Rad52 fused to a thioredoxin and a 6X polyhistidine tag. Dynamic and static light scattering tested the construct and its complex with RPA 14/32 heterodimer and RPA heterotrimer.

#### **Construction of a C-terminal fragment of Rad52 with RPA binding activity.**

The N-terminal region of Rad52 (from residues 1 to 192) is required for the DNA binding activity and the formation of a heptameric ring structure (see appendix reference #1). The results from specific aim 1 show the formation of the RPA/Rad52 complex has multiple sites for its interaction. Both on the 70 and 32 kDa subunit, are surfaces for Rad52 binding. Both subunits bind between the region of 218-303 which is beyond the heptameric self-association domain and DNA binding domain of Rad52. During the course of this fellowship, the Rad52 C-terminal region was cloned, expressed, purified to homogeneity suitable for the production of X-ray quality crystals. The highlights include:

- 1) The C-terminal region of Rad52 from residues 218-418 was PCR amplified, cloned into a pET28a vector as a fusion protein with an N-terminal thioredoxin and 6X polyhistidine tag.
- 2) The Rad52 (218-418) construct was purified to homogeneity by a three step protocol after lysis which included immobilized metal chelate chromatography, HQ chromatography, and Superdex 200 (Gel filtration) chromatography. Typical prep results are included in figure 3.
- 3) Solution conditions for the Rad52(218-418) were probed using dynamic light scattering to promote monodispersity of the protein. In the dynamic light scattering studies of free Rad52(218-418), it was found that high pH (around pH=10) and the presence of a small amount of detergent (n-hexyl-glucopyranoside) promote a monomodal and a near monodisperse solution (Cp/Rh of 22% and a baseline value of 1.000).

### **Specific aim 3- To determine solution conditions which favor the interaction between RPA and Rad52 and promote crystallization.**

Solution conditions for the RPA/Rad52 fragment complex were determined by using an ELISA protocol as well as dynamic and static light scattering. Significant crystallization variables were screened such as pH, concentration, detergents, mono and divalent cations, organic compounds. The main results obtained are listed here:

- 1) Using an ELISA protocol, which was modified to probe conditions such as ionic strength, we have shown that the Rad52/RPA complex has an association maximum at low ionic strength <150 mM (see appendix reference #3).
- 2) Using dynamic light scattering and static light scattering, we were able to show that the minimum amount of polydispersity is formed at a stoichiometric ratio of 1:1 (see appendix reference #3; experimental section).
- 3) Maximum formation of the complex occurs between pH= 7.8 and 8.5 (shown by ELISA and dynamic light scattering ; unpublished preliminary data).
- 4) The Rad52(218-418) /RPA 14/32 complex is polydisperse in solution whereas the Rad52(218-418)/RPA complex has lower polydispersity than the Rad52(218-418) alone (see appendix reference #3; static light scattering).
- 5) The formation of the Rad52/RPA complex has a 1:1 stoichiometry (see appendix reference #3; size analysis of Rad52/RPA complexes).

### **Specific aim 4&5- Obtain diffraction quality crystals of the RPA/Rad52 complex and solve the phase problem, structure of the complex.**

No success has been found in the attempts to crystallize the Rad52(218-418)/RPA 14/32 complex or the Rad52(218-418)/RPA complex. We have found a condition that forms crystals for the Rad52(218-418) alone. A photograph of the crystal and condition is shown below:



**Figure 1-** A picture of a crystal of Rad52(218-418) alone. The crystal grew in: 20% PEG 3350, 200 mM ammonium fluoride, .5 mM n-hexyl-glucopyranoside, 2% glycerol, 500 mM KCl. The measure pH of the mother liquor was 9.2. The crystallization time took 9 months. The diffraction characteristics of the crystal is currently being investigated.

## Key research accomplishments

Key research accomplishments are listed within the specific aim:

- 1) We have determined minimum interacting regions for Rad52 and RPA.
- 2) Optimized purification protocols for RPA, RPA 14/32, Rad52, Rad52(218-418) that are suitable for crystal screening and crystal growth.
- 3) Determined solution conditions for Rad52(218-418) and Rad52(218-418)/RPA complex with minimum amount of aggregation and suitable for crystal screening and crystal growth.
- 4) Maximized the binding interaction between Rad52 and RPA by minimizing ionic strength.
- 5) Helped determine a second mode of self-association for Rad52 which a domain is located on the C-terminal half of Rad52 (found on wild-type and Rad52(218-418); appendix reference #1) that mediates this interaction.
- 6) Helped determine the nature of the thermal stability of Rad52 (Rad52 and the N-terminal region of Rad52 maintains high thermal stability whereas the C-terminal half unfolds at low temperature).
- 7) Characterized the ionic nature of the Rad52/RPA complex and the electrostatic potential of the interacting surfaces (see appendix reference #3).
- 8) Determined the molecular stoichiometry of the Rad52/RPA complex using dynamic and static light scattering (see appendix reference #3).
- 9) We were the first to show (with the help of Dr. Marc Wold, University of Iowa) that protein interactions between RPA and other interacting protein (either Rad52 or the many other proteins that interact with RPA) can modulate the ssDNA affinity of RPA. In contrast to this accomplishment, our preliminary results point to a cross-communication of Rad52, RPA32, RPA70 and ssDNA (see appendix reference #3).

## Reportable outcomes

### Publications:

Ranatunga W., **Jackson D.**, Lloyd J., Forget A., Knight K., Borgstahl G., *Human Rad52 exhibits two modes of self association*, J. Biol. Chem. (2001) 276(19), p15876

Ranatunga W., **Jackson D.**, Flowers R., Borgstahl G., *Human Rad52 has high thermal stability*, Biochemistry, 2001, 40, 8557

**Jackson D.**, Dahr K., Wahl J., Wold MS., Borgstahl GEO., *Analysis of the human replication protein A/ Rad52 complex: evidence for crosstalk between RPA32, RPA70, Rad52 and DNA*, J. Mol. Biol., (2002) 321, 133-148

### Lecture Presentations:

**Jackson D.**, *Characterization of the Rad52/RPA protein-protein interaction*, (presented at the **Sigma Xi** symposium on 5/20/01)

### Poster Presentations:

**Jackson D.**, Ranatunga W., Lloyd J., Forget A., Knight K., Borgstahl G. *The self association of the C-terminal half of human Rad52 and its interaction with human RPA* ( presented at the 15<sup>th</sup> annual Protein Society symposium on July 2001, vol. 10, suppl 2, #346; this poster also received a Finn Wold travel award)

## Conclusions

We have completed the first three specific aims of the fellowship goals. We regret not accomplishing the fourth and fifth specific aim of this fellowship. Our accomplishment is the large wealth of knowledge obtained about the nature of the Rad52/RPA complex.

## Human RAD52 Exhibits Two Modes of Self-association\*

Received for publication, December 27, 2000  
Published, JBC Papers in Press, February 13, 2001, DOI 10.1074/jbc.M011747200

Wasantha Ranatunga<sup>‡§</sup>, Doba Jackson<sup>‡§</sup>, Janice A. Lloyd<sup>§¶</sup>, Anthony L. Forget<sup>§¶</sup>, Kendall L. Knight<sup>¶</sup>, and Gloria E. O. Borgstahl<sup>¶</sup>

From the <sup>‡</sup>Department of Chemistry, University of Toledo, Toledo, Ohio 43606-3390 and the <sup>¶</sup>Department of Biochemistry and Molecular Pharmacology, University of Massachusetts Medical School, Worcester, Massachusetts 01655-0103

The human RAD52 protein plays an important role in the earliest stages of chromosomal double-strand break repair via the homologous recombination pathway. Individual subunits of RAD52 self-associate into rings that can then form higher order complexes. RAD52 binds to double-strand DNA ends, and recent studies suggest that the higher order self-association of the rings promotes DNA end-joining. Earlier studies defined the self-association domain of RAD52 to a unique region in the N-terminal half of the protein. Here we show that there are in fact two experimentally separable self-association domains in RAD52. The N-terminal self-association domain mediates the assembly of monomers into rings, and the previously unidentified domain in the C-terminal half of the protein mediates higher order self-association of the rings.

The repair of double-strand breaks in chromosomal DNA is of critical importance for the maintenance of genomic integrity. In *Saccharomyces cerevisiae*, genes of the RAD52 epistasis group, RAD50, RAD51, RAD52, RAD54, RAD55, RAD57, RAD59, MRE11, and XRS2, were identified initially by the sensitivity of mutants to ionizing radiation (1, 2). These genes have been implicated in an array of recombination events including mitotic and meiotic recombination as well as double-strand break repair. RAD52 mutants show the most severe pleiotropic defects suggesting a critical role for the protein in homologous recombination and double-strand break repair (2). The importance of specific protein-protein interactions in the catalysis of homologous recombination is suggested by studies demonstrating specific contacts and functional interactions between Rad52p and a number of proteins involved in recombination including Rad51p (3–8), which catalyzes homologous pairing and strand exchange, and replication factor A (RPA)<sup>1</sup> (8–10), a heterotrimeric single-stranded DNA binding protein (11).

\* This work was supported by the United States Army Medical Research and Materiel Command under DAMD17-98-1-8251 (to G. E. O. B.) and National Institutes of Health Grant GM44772 (to K. L. K.). Brookhaven National Laboratory STEM is supported by National Institutes of Health Grant P41-RR01777 and partially supported by the Department of Energy and Office of Biological and Environmental Research. The costs of publication of this article were defrayed in part by the payment of page charges. This article must therefore be hereby marked "advertisement" in accordance with 18 U.S.C. Section 1734 solely to indicate this fact.

§ These authors contributed equally to this work.

¶ To whom correspondence should be addressed: Dept. of Chemistry, University of Toledo, 2801 W. Bancroft St., Toledo, OH 43606-3390. Tel.: 419-530-1501; Fax: 419-530-4033; E-mail: gborgst@uoft02.utoledo.edu.

<sup>1</sup> The abbreviations used are: RPA, replication protein A; MES, 4-morpholineethanesulfonic acid; EM, electron microscopy; STEM, scanning transmission electron microscopy; BSA, bovine serum albumin; DLS, dynamic light scattering.

Studies of the equivalent human proteins have identified similar interactions between the RAD52, RAD51, and replication protein A proteins (12–17). Based on a series of protein-protein interaction assays (15, 16, 18) and DNA binding studies<sup>2</sup> (16), a domain map of RAD52 was proposed by Park *et al.* (16) (see Fig. 1). The determinants of self-association were proposed to exist exclusively within a region defined by residues 65–165, a result supported by recent studies of several isoforms of RAD52 (19). Electron microscopy (EM) studies of Rad52p and RAD52 have revealed formation of ring-shaped structures (9–13 nm in diameter), as well as higher order aggregates (9, 12, 20). Stasiak *et al.* (21) performed image analyses of negatively stained electron micrographs and determined that the 10-nm RAD52 rings are composed of seven subunits. Scanning transmission electron microscopy (STEM) analysis indicated a mean mass of  $330 \pm 59$  kDa supporting a heptameric ring-shaped RAD52 structure (21). Recent studies show that RAD52 binds to double-stranded DNA ends as an aggregated complex (20). These end-binding complexes were amorphous in shape and ranged in size from 15 to 60 nm. Within these complexes, RAD52 rings were observed occasionally. Binding of RAD52 to the DNA ends promoted end-to-end association between DNA molecules and stimulated ligation of both cohesive and blunt DNA ends (20).

Therefore, given that the formation of both ring-shaped oligomers and aggregates of these rings seem relevant to RAD52 function, we sought to investigate further the self-association properties of the RAD52 protein. We performed a series of analyses comparing full-length RAD52 (1–418) with two different mutant RAD52 proteins: (i) a 1–192 mutant that spans the N-terminal portion and includes the entire proposed DNA binding and self-association domains and (ii) a 218–418 mutant that spans the C-terminal portion of RAD52 that includes the proposed RPA- and RAD51-binding domains (Fig. 1). In contrast to previous studies, our results show that there are experimentally separable determinants for two different modes of self-association by RAD52, one in the N-terminal and one in the C-terminal portion of the protein.

### EXPERIMENTAL PROCEDURES

**RAD52 Constructs**—Wild-type RAD52 and RAD52 (1–192) pET28 expression plasmids were a gift from Dr. M. Park and have six histidines fused to the C terminus. A pET28 expression plasmid containing the thioredoxin-RAD52 (218–418) fusion protein was constructed using standard polymerase chain reaction techniques.

**Protein Purification**—Cultures of transformed BL21(DE3) Codon Plus *Escherichia coli* (Stratagene) were grown in a fermentor and induced with 0.5 mM isopropyl-1-thio- $\beta$ -D-galactopyranoside. Wild-type RAD52 and RAD52 (1–192) cells were resuspended in a buffer consisting of 20 mM HEPES, pH 6.0, 10% glycerol, 400 mM NaCl, 100 mM KCl, 5 mM  $\beta$ -mercaptoethanol, 1 mM dithiothreitol, 1 mM hexylglucopyranoside, and 1 mM EDTA. RAD52 (218–418) cells were resuspended in a

<sup>2</sup> J. A. Lloyd, and K. L. Knight, unpublished data.



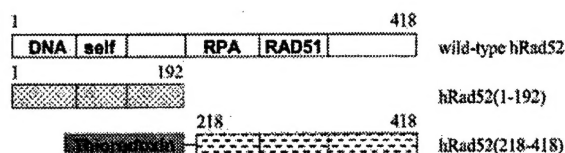


**FIG. 1. Schematic diagram of wild-type RAD52 and deletion mutants.** The beginning and ending residue numbers of each mutant are indicated along with domain structure. The following domains and residue numbers were defined by Park *et al.* (16): DNA binding, 39–80; self-association, 85–159; RPA binding, 221–280; RAD51 binding, 290–330.

buffer consisting of 50 mM HEPES, pH 8, 500 mM KCl, 500 mM LiSO<sub>4</sub>, 2.5% glycerol, 1 mM EDTA, 5 mM dithiothreitol, 4 mM imidazole, and 0.1% Triton X-100. Protease inhibitors (1 mM phenylmethylsulfonyl fluoride and 10 mM benzamide) were used throughout purification. Cells were lysed using a French press, and the lysate was clarified by centrifugation, filtration through Cell Debris Remover-modified cellulose (Whatman), and passage through a 0.22- $\mu$ m pore filter. The clarified lysate was applied to an MC/M Ni<sup>2+</sup> affinity column (PerSeptive Biosystems) that was optimally washed and eluted with an imidazole gradient. Wild-type RAD52 and RAD52(1–192) then were dialyzed extensively against a buffer consisting of 20 mM MES, pH 6.0, 10% glycerol, 400 mM NaCl, 100 mM KCl, 5 mM  $\beta$ -mercaptoethanol, 1 mM dithiothreitol, 1 mM hexylglucopyranoside, and 1 mM EDTA. RAD52(218–418) was dialyzed extensively against a buffer consisting of 50 mM HEPES, pH 8.0, 2.5% glycerol, 2.5 mM EDTA, and 0.5 mM hexylglucopyranoside and then purified further by anion exchange using an HQ/M column (PerSeptive Biosystems) eluted with a KCl gradient. Protein samples were concentrated using Amicon concentrators with YM10 membranes, and protein concentrations were determined using Bradford assay (Bio-Rad) with bovine serum albumin (BSA) as a standard. The expression plasmid for wild-type RPA heterotrimer was a gift from Dr. M. Wold. RPA was expressed and purified as described (22).

**Enzyme-linked Immunosorbent Assay**—The enzyme-linked immunosorbent assay was done at room temperature. Briefly, 10 pmol of wild-type RAD52, RAD52 mutants, or BSA were coated to microtiter plates for 1 h. Plates were washed three times with phosphate-buffered saline (PBS) containing 0.02% Tween 20 to remove unbound protein. Plates then were blocked with 5% milk in PBS for 10 min and then washed. Various amounts of RPA in PBS and 5% milk were added and incubated for 1 h. Plates then were washed to remove nonspecific interactions and probed with a monoclonal antibody against the 70-kDa subunit of RPA (Calbiochem) in PBS and 5% milk for 30 min. Plates then were washed and probed with anti-mouse IgG peroxidase conjugate (Sigma) in PBS and 5% milk for 30 min and washed. Plates were developed using 3,3',5,5'-tetramethylbenzidine in phosphate-citrate buffer with 0.03% hydrogen peroxide. Color was developed for 30 min, the reaction was stopped with 1.5 M H<sub>2</sub>SO<sub>4</sub>, and absorbance readings at 450 nm were taken with a microtiter plate reader. Background absorbance was determined from a blank well and then subtracted from the data.

**Gel-shift DNA Binding Assays**—Reactions (20  $\mu$ l) contained 20 mM triethanolamine-HCl, pH 7.5, 1 mM dithiothreitol, 1 mM MgCl<sub>2</sub>, 0.1 mg/ml BSA, 0.05% Tween 20, 2 mM 5'-end-labeled 95 base oligonucleotide (concentration in bases), and the indicated amounts of protein. The oligonucleotide sequence is as follows: 5'-AGA CGA TAG CGA AGG CGT AGC AGA AAC TAA CGA AGA TTT TGG CGG TGG TCT GAA CGA CAT CTT TGA GGC GCA GAA AAT CGA GTG GCA CTA ATA AG-3'. Reactions were incubated at 37 °C for 20 min followed by the addition of glutaraldehyde to 0.2% and continued incubation at 22 °C for 20 min. Glycerol was added to a final concentration of 1.6% (w/v) and samples (10  $\mu$ l) were loaded onto a 0.8% agarose gel and electrophoresed at 100 mV in 0.5 $\times$  TBE buffer (90 mM Tris, 64.6 mM boric acid, and 2.5 mM EDTA, pH 8.3). Gels were analyzed using a Molecular Imager FX and QuantityOne software (Bio-Rad). The 95-base oligonucleotide used in the gel-shift assays was made using an ABI 392 DNA/RNA synthesizer.

**Dynamic Light-scattering (DLS) Analysis**—DLS was carried out using a DynaPro-801 molecular sizing instrument equipped with a micro-sampler (Protein Solutions). A 50- $\mu$ l sample was passed through a filtering assembly into a 12- $\mu$ l chamber quartz cuvette. For RAD52(1–192) and RAD52(218–418), 20-nm filters were used. For wild-type RAD52, a 100-nm filter was used. The data were analyzed first using Dynamics 4.0 software and then DynaLS software as follows. Hydrodynamic radii ( $R_h$ ) for monomodal distributions, as defined by a baseline ranging from 0.977 to 1.002, were reported from Dynamics 4.0. Bi- and multimodal distributions were analyzed using DynaLS. DynaLS data estimates of molecular weight were obtained from  $R_h$  using Dy-

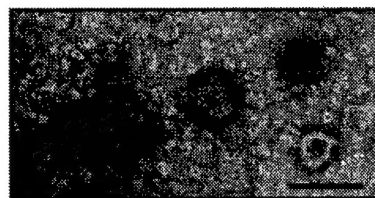


**FIG. 2. Negative stained electron micrograph of wild-type RAD52.** Wild-type RAD52 (4.0  $\mu$ M) was prepared as described under "Experimental Procedures." Larger spherical particles are ~80 nm in diameter, half-spheres are 50 nm, and numerous 10-nm rings are visible also. Black bar = 0.1  $\mu$ m.

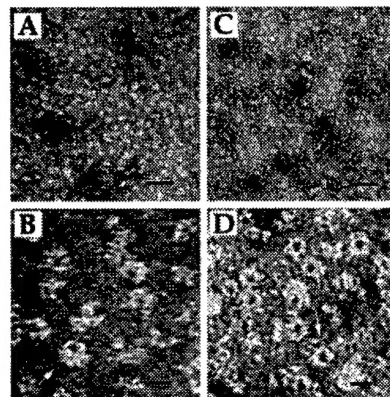


**FIG. 3. Negative stained electron micrographs of wild-type RAD52 and RAD52(1–192) protein.** Proteins (4.0  $\mu$ M) were prepared as described under "Experimental Procedures." The majority of protein for both wild-type RAD52 (A and B) and RAD52(1–192) (C and D) forms 10-nm diameter ring-shaped oligomers. Larger particles of wild-type RAD52 in A (also see Fig. 2) are not formed by RAD52(1–192). Higher magnifications of both proteins reveal that the protrusions observed on the 10-nm rings of wild-type RAD52 are missing in the RAD52(1–192) rings (arrows in B and D). Black bars = 0.05  $\mu$ m in A and C and 0.01  $\mu$ m in B and D.

namics 3.0 molecular weight calculator. Sum of squares errors less than 5000 were considered negligible.

**Electron Microscopy**—Proteins were prepared for EM by diluting wild-type or mutant RAD52 to 4.0  $\mu$ M in a buffer containing 20 mM Tris-HCl, pH 7.5, 5% glycerol, 5 mM  $\beta$ -mercaptoethanol, 0.1 mM EDTA, and 100 mM KCl. Samples were spread onto thin carbon films on holey carbon grids (400 mesh), stained with 1% uranyl acetate, and visualized by transmission electron microscopy using a Philips CM10 microscope.

**STEM Analysis**—Analyses were carried out at the Brookhaven National Laboratory using unstained, unshadowed freeze-dried samples. Protein samples (~0.1 mg/ml) were applied to a thin carbon film supported by a thick holey film on titanium grids and freeze-dried overnight. The microscope operates at 40 kV. Operation of the STEM and data analyses were performed as described previously (23).

**Gel Filtration**—Samples of the RAD52(218–418) protein at 1.2 mg/ml were loaded onto a Superdex 200 HR 10/30 gel filtration column (Amersham Pharmacia Biotech/LKB) equilibrated in buffer containing 20 mM MES, pH 6.0, 400 mM NaCl, 100 mM KCl, 10% (w/v) glycerol, 5 mM  $\beta$ -mercaptoethanol, and 1 mM EDTA. Analysis was performed using a BioLogic chromatography system (Bio-Rad) with an in-line UV detector.

## RESULTS

**Oligomeric Characteristics of RAD52 Proteins**—EM analyses of wild-type RAD52 and RAD52(1–192) show that both proteins form ring-shaped structures (Figs. 2 and 3). The average diameter of these particles, measured across the surface with the central pore, is  $10 \pm 1$  nm, consistent with previous reports (9, 12, 21). Wild-type RAD52 also forms distinct larger particles that appear as various sized spheres and half-spheres ranging in diameter from 30 to 100 nm (Fig. 2). These particles consist of individual 10-nm rings as well as other less distinct com-

**FIG. 4. STEM histograms.** STEM mass analyses were performed as described under "Experimental Procedures." Histograms include pooled data from several separate analyses (eight for wild-type RAD52, six for RAD52-(1-192), and five for RAD52-(218-418)). Average mass values were as follows: A, wild-type RAD52  $298 \pm 69$  kDa ( $n = 309$ ); B, RAD52-(1-192)  $227 \pm 30$  kDa ( $n = 277$ ); C, RAD52-(218-418)  $153 \pm 40$  kDa ( $n = 119$ ).

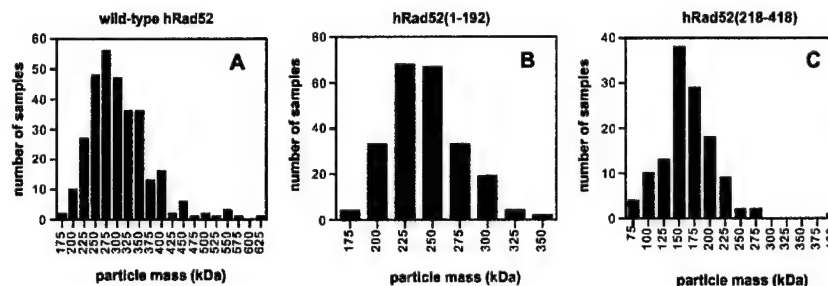


**TABLE I**  
Dynamic light-scattering measurements of RAD52 proteins

Protein	Concentration	Base line	Modality	SOS <sup>a</sup>	$R_H^b$	Molecular mass	Peak <sup>c</sup> area
	mg/ml			error	nm	kDa	%
RAD52	3.5	1.007	Multimodal	3.10	6.6 (0.7) 27.6 (9.3) 711.0 (245)	279 $9.05 \times 10^3$ $2.40 \times 10^7$	10.5 85.8 3.7
RAD52-(1-192)	15	1.001	Monomodal	1.95	5.7 (1.2)	200	
RAD52-(218-418)	2	1.001	Monomodal	0.64	4.6 (2.1)	118	
Thioredoxin	1	1.001	Monomodal	3.3	2.0 (0.8)	14.8	

<sup>a</sup> SOS, sum of squares.

<sup>b</sup> Average hydrodynamic radius ( $R_H$ ) is reported with the polydispersity (width of the distribution in nm) given in parentheses.

<sup>c</sup> For DynaLS results the percent peak area for the solvent peak is not reported.

pressed structures. For RAD52-(1-192) the majority of protein forms ring-shaped oligomers, and no larger particles were seen (Fig. 3). Even at increased concentrations (6 and 10  $\mu$ M) RAD52-(1-192) shows no larger aggregates (data not shown). Higher magnifications reveal "protrusions" extending from the 10-nm rings formed by wild-type RAD52 that are missing in the 1-192 protein (see arrows in Fig. 3, B and D). These protrusions likely correspond to those modeled by Stasiak *et al.* (21), and our data show that they are part of the C-terminal portion of RAD52.

STEM analyses of wild-type RAD52 (2  $\mu$ M) showed particle sizes ranging from 175 to 625 kDa with a mass average of  $298 \pm 69$  kDa ( $n = 309$ ; Fig. 4A). Given a molecular mass of 48 kDa for the His-tagged RAD52 protein, this range corresponds to particles that contain from 4 to 13 subunits with an average of six subunits. Similar analyses of the 1-192 protein showed particle sizes ranging from 100 to 350 kDa with a mass average of  $227 \pm 30$  kDa ( $n = 277$ ; Fig. 4B). For a monomer molecular mass of 23 kDa, this range corresponds to particles that contain from 4 to 15 subunits with an average of 10 subunits. Resolution of the ring-shaped oligomers in the electron micrographs was not high enough to count individual subunits, but our STEM data are consistent with previous work in which oligomeric rings of wild-type RAD52 were determined to be heptameric (21).

The oligomeric distribution of these proteins in solution was investigated by DLS. Wild-type RAD52 shows a multimodal profile with three peaks corresponding to particles with an average hydrodynamic radius of 6.6, 27.6, and 711.0 nm, respectively (Table I). These likely correspond to ring-shaped oligomers, the 30-nm particles described previously as "super-rings" (12) and seen in our micrographs (Fig. 2), and larger aggregates also observed in our micrographs. We find that the percent distribution of these various sized particles is effected by protein concentration, *i.e.* with increasing concentration the larger aggregates account for a larger percentage of the population. In contrast to wild type, RAD52-(1-192) shows a monomodal light-scattering profile that corresponds to a particle with a hydrodynamic radius of 6.1 nm (Table I), which is in agreement with our EM analysis.

The above analyses indicate at least two modes of RAD52 self-association that are experimentally separable, (i) forma-

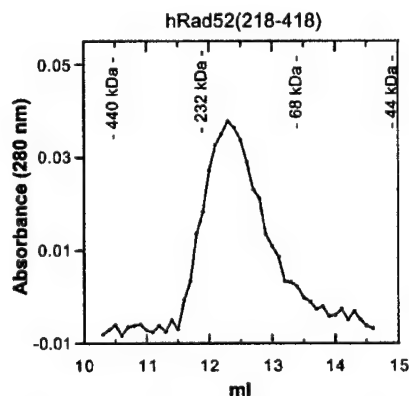
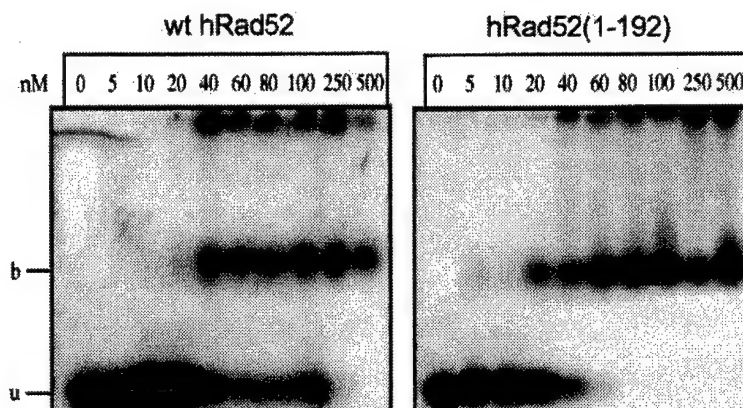


**FIG. 5. Gel filtration profile of the thioredoxin-218-418 fusion RAD52 protein.** The mutant protein (1.2 mg/ml, 35.8  $\mu$ M) was loaded onto a Superdex 200 HR 10/30 gel filtration column, and elution of protein was followed at  $A_{280\text{ nm}}$ . The indicated elution volumes of standards (ferritin, 440 kDa; catalase, 232 kDa; BSA, 68 kDa; ovalbumin, 44 kDa) were an average of four runs.

tion of ring-shaped oligomers and (ii) formation of larger aggregates. Because the latter seems to depend largely on the presence of residues C-terminal to position 192, we performed a number of assays to test for self-association on a mutant RAD52 containing only residues 218-418. Initial EM studies showed no distinct structural characteristics for this protein (data not shown), but STEM analysis revealed particle sizes ranging from 75 to 275 kDa (Fig. 4C) with a mass average of  $153 \pm 40$  kDa ( $n = 119$ ; Fig. 4C). Given a monomer molecular mass of 39 kDa, the particle composition ranges from two to seven subunits with an average of four subunits. Gel filtration shows a homogeneous peak corresponding to a molecular mass of 166 kDa (Fig. 5) and therefore to a particle containing approximately four subunits. Analysis by DLS shows a monomodal peak corresponding to a particle with an average  $R_H$  of 4.6 nm and a molecular mass of 118 kDa (therefore containing approximately three subunits). DLS measurements on thioredoxin alone show that it does not contribute to the oligomeric character of thioredoxin-RAD52-(218-418) (Table I). Together,

**FIG. 6. Gel-shift DNA Binding assays.** Indicated concentrations of either wild-type RAD52 or RAD52-(1-192) were incubated with a 5'-end-labeled 95-base oligonucleotide followed by cross-linking with glutaraldehyde as described under "Experimental Procedures." Reactions were electrophoresed on a 0.8% agarose gel. Radioactive material at the top of the gel represents protein-DNA complex trapped in the gel well. *u*, unbound DNA; *b*, protein-DNA complex.



these data indicate that the C-terminal portion of RAD52 (residues 218-418) contains determinants of protein self-association that are distinct from those required to form 10-nm rings.

**DNA Binding**—Binding of wild-type RAD52 and RAD52-(1-192) to single-stranded DNA was analyzed by gel-shift assays. The gels in Fig. 6 are representative of five different experiments, each of which gave similar results. In each case, analysis of unbound and bound DNA (including that in the gel well) gave rise to a  $K_{D(app)}$  of 35 and 25 nM for wild-type RAD52 and RAD52-(1-192), respectively. This slight enhancement in binding affinity was observed consistently for RAD52-(1-192). With wild-type RAD52 a significant portion of bound DNA remained in the gel well, a result that likely reflects the ability of the wild-type protein to form greater amounts of self-aggregates than the 1-192 mutant protein (see below). Additionally, 100% of the DNA (2 nM total nucleotides) was bound by the 1-192 protein at 40-60 nM protein in the titration profile, whereas 100% binding by wild-type RAD52 consistently required greater than 100 nM protein. Assays using the RAD52-(218-418) mutant protein showed no DNA binding up to 2.0  $\mu$ M protein (data not shown). These results show that the DNA binding domain of RAD52 is contained within the N-terminal portion of the protein and that removal of the C-terminal 227 residues results in a slight enhancement of DNA binding.

**Interaction of RAD52 Proteins with RPA**—Previous studies have mapped residues 221-280 as the domain in RAD52 that interacts with the 32-kDa subunit of RPA (16). To ensure that the 218-418 mutant construct maintained a native fold, we tested this protein for interaction with RPA using an immunosorbent assay. Enzyme-linked immunosorbent assays showed that the 218-418 protein interacted with RPA with an affinity similar to that observed for wild-type RAD52 (Fig. 7). No interaction with RPA was observed for RAD52-(1-192), thioredoxin, or BSA.

#### DISCUSSION

Previous studies have shown that RAD52 exists in a number of oligomeric states ranging from rings with a 10-nm diameter to larger complexes with diameters of greater than 30 nm (9, 12, 20, 21). Recent observations indicate a direct role for these higher order protein-protein interactions in promoting DNA end-joining (20). We therefore sought to investigate the self-association properties of RAD52 utilizing an array of biophysical techniques.

In our EM studies of wild-type RAD52 and RAD52-(1-192), we observed ring structures with an average diameter of  $10 \pm 1$  nm as has been reported previously (9, 12, 20, 21). Additionally, and as seen previously (12, 20, 21), we observed protrusions extending from wild-type RAD52 rings as well as a population of distinct larger particles. However, neither the protrusions nor the larger particles were observed with RAD52-(1-192). This suggests that

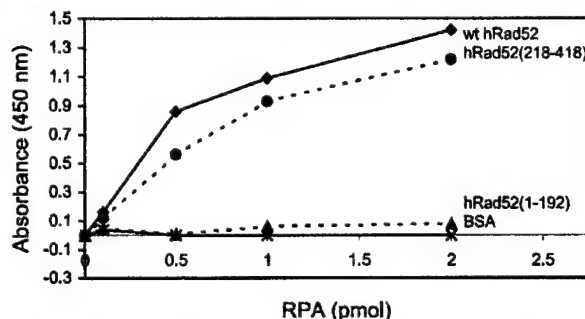


**FIG. 7. RAD52-RPA protein-protein interactions.** Enzyme-linked immunosorbent assays were performed as described under "Experimental Procedures" with RAD52 proteins immobilized to microtiter plates and probed with increasing amounts of RPA heterotrimer. The experiment was performed in triplicate, and the average for each RPA concentration was plotted. The error was on the order of 5-10%. *wt*, wild type.

residues within the C-terminal portion of the protein (residues 193-418) make up these protrusions and carry determinants for higher order RAD52 self-association.

DLS analysis of wild-type RAD52 and the two mutant proteins provides additional and complementary evidence for two distinct modes of RAD52 self-association. DLS analysis of wild-type RAD52 shows three peaks that likely correspond to the 10-nm ring-shaped oligomers and the 30-nm and larger particles observed by EM. In contrast, both RAD52-(1-192) and RAD52-(218-418) show a monomodal DLS profile indicating the presence of a single population of structures. The RAD52-(1-192)  $R_H$  is consistent with a ring structure, and the RAD52-(218-418)  $R_H$  indicates a complex composed of three subunits. This self-association of RAD52-(218-418) was confirmed by size-exclusion chromatography and STEM.

The ability of RAD52-(218-418) to self-associate was unexpected. Previous studies have suggested that residues 65-165 define the exclusive self-association domain in the RAD52 protein (18). Shen *et al.* (18) found that although N-terminal fragments of the protein self-associated in two-hybrid screens and affinity chromatography assays, fragments containing various portions of the C terminus, *e.g.* 287-418 or 166-418, did not. In contrast to these results, we find that RAD52-(218-418) is able to self-associate. Although our EM analysis revealed no distinct oligomeric structures for RAD52-(218-418), three different methods (STEM, gel filtration, and DLS) showed that this mutant formed oligomeric particles containing 3-4 subunits. These data for RAD52-(218-418), coupled with the inability of RAD52-(1-192) to form structures larger than the 10-nm rings, indicate that residues within the C-terminal region of the pro-



tein make important contributions to RAD52 self-association. Thus, the C-terminal region of RAD52 contains a novel self-association domain distinct from that previously identified within residues 65–165 (18).

Importantly, functional analyses of both the 1–192 and 218–418 mutant proteins show that each maintains an expected activity. Both wild-type RAD52 and the 1–192 proteins, which form ring-shaped oligomers, bound single-stranded DNA with similar affinities. This is consistent with previous studies that mapped the DNA binding domain of RAD52 to residues 39–80<sup>2</sup> (16). The elevated affinity of RAD52-(1–192) for single-stranded DNA was noted also for a similar Rad52p construct (24). Also as expected, RAD52-(218–418) showed a specific interaction with RPA. Again, this is consistent with previous studies that mapped the RPA interaction domain to residues 221–280 in RAD52 (16). The fact that both mutant proteins showed the expected functions demonstrates that they very likely maintain native structure, thereby supporting the relevance of differences observed in their oligomeric characteristics compared with wild-type RAD52.

In summary, our data support a model in which the self-association domain within the N-terminal region of RAD52 (residues 1–192) promotes the formation of ring-shaped oligomers that are functional for DNA binding, whereas the C-terminal domain (residues 218–418) mediates higher order self-association events. Additionally, the protrusions extending from the 10-nm ring structure of wild-type RAD52, originally modeled by Stasiak *et al.* (21) and seen clearly in our electron micrographs, correspond to the C-terminal region of the protein. Given the likely importance of higher order self-association to the ability of RAD52 to promote end-to-end joining of DNA breaks (20), these protrusions seem to mediate a critically important aspect of RAD52 function. Further studies of various mutant RAD52 proteins will clarify the contribution made by the different aspects of self-association toward the overall function of this important DNA repair protein.

**Acknowledgments**—We thank Matt Pokross and Jeff Habel for technical assistance and Krishnamurthy Rajeswari and Cathy Schellert for help in the early stages of this project. We also thank Dr. Min Park at Los Alamos National Laboratory for wild-type RAD52 and RAD52-(1–192) expression plasmids. We gratefully acknowledge Dr. Martha Simon at Brookhaven National Laboratory for performing the STEM analyses.

#### REFERENCES

1. Game, J., and Mortimer, R. K. (1974) *Mutat. Res.* **24**, 281–292
2. Petes, T. D., Malone, R. E., and Symington, L. S. (1991) in *The Molecular and Cellular Biology of the Yeast, Saccharomyces* (Broach, J. R., Pringle, J. R., and Jones, E. W., eds) pp. 407–522, Cold Spring Harbor Laboratory Press, Cold Spring Harbor, NY
3. Shinohara, A., and Ogawa, T. (1998) *Nature* **391**, 404–407
4. Milne, G. T., and Weaver, D. T. (1993) *Genes Dev.* **7**, 1755–1765
5. Hays, S. L., Firmenich, A. A., and Berg, P. (1995) *Proc. Natl. Acad. Sci. U. S. A.* **92**, 6925–6929
6. Johnson, R. D., and Symington, L. S. (1995) *Mol. Cell. Biol.* **15**, 4843–4850
7. Sung, P. (1997) *J. Biol. Chem.* **272**, 28194–28197
8. New, J. H., Sugiyama, T., Zaitseva, E., and Kowalczykowski, S. C. (1998) *Nature* **391**, 407–410
9. Shinohara, A., Shinohara, M., Ohta, T., Matsuda, S., and Ogawa, T. (1998) *Genes Cells* **3**, 145–156
10. Sugiyama, T., New, J. H., and Kowalczykowski, S. C. (1998) *Proc. Natl. Acad. Sci. U. S. A.* **95**, 6049–6054
11. Wold, M. S. (1997) *Annu. Rev. Biochem.* **66**, 61–91
12. Van Dyck, E., Hajibagheri, N. M. A., Stasiak, A., and West, S. C. (1998) *J. Mol. Biol.* **284**, 1027–1038
13. Golub, E. I., Gupta, R. C., Haaf, T., Wold, M. S., and Radding, C. M. (1998) *Nucleic Acids Res.* **26**, 5388–5393
14. Baumann, P., and West, S. C. (1999) *J. Mol. Biol.* **291**, 363–374
15. Shen, Z., Cloud, K. G., Chen, D. J., and Park, M. S. (1996) *J. Biol. Chem.* **271**, 148–152
16. Park, M. S., Ludwig, D. L., Stigger, E., and Lee, S. H. (1996) *J. Biol. Chem.* **271**, 18996–19000
17. Benson, F. E., Baumann, P., and West, S. C. (1998) *Nature* **391**, 401–404
18. Shen, Z., Peterson, S. R., Comeaux, J. C., Zastrow, D., Moyzis, R. K., Bradbury, E. M., and Chen, D. J. (1996) *Mutat. Res.* **364**, 81–89
19. Kito, K., Wada, H., Yeh, E. T., and Kamitani, T. (1999) *Biochim. Biophys. Acta* **1489**, 303–314
20. Van Dyck, E., Stasiak, A. Z., Stasiak, A., and West, S. C. (1999) *Nature* **398**, 728–731
21. Stasiak, A. Z., Larquet, E., Stasiak, A., Muller, S., Engel, A., Dyck, E. V., West, S. C., and Egelman, E. H. (2000) *Curr. Biol.* **10**, 337–340
22. Henriksen, L. A., Umbricht, C. B., and Wold, M. S. (1994) *J. Biol. Chem.* **269**, 11121–11132
23. Wall, J. S., Hainfeld, J. F., and Simon, M. N. (1998) *Methods Cell Biol.* **53**, 139–164
24. Mortensen, U. H., Bendixen, C., Sunjevaric, I., and Rothstein, R. (1996) *Proc. Natl. Acad. Sci. U. S. A.* **93**, 10729–10734

Human RAD52 Protein Has Extreme Thermal Stability<sup>†</sup>

Wasantha Ranatunga, Doba Jackson, Robert A. Flowers II, and Gloria E. O. Borgstahl\*

Department of Chemistry, The University of Toledo, Toledo, Ohio 43606-3390

Received February 2, 2001; Revised Manuscript Received April 27, 2001

**ABSTRACT:** The human RAD52 protein plays an important role in the earliest stages of chromosomal double-strand break repair via the homologous recombination pathway. Individual subunits of RAD52 associate into seven-membered rings. These rings can form higher order complexes. RAD52 binds to DNA breaks, and recent studies suggest that the higher order self-association of the rings promotes DNA end joining. Monomers of the RAD52(1–192) deletion mutant also associate into ring structures but do not form higher order complexes. The thermal stability of wild-type and mutant RAD52 was studied by differential scanning calorimetry. Three thermal transitions (labeled A, B, and C) were observed with melting temperatures of 38.8, 73.1, and 115.2 °C. The RAD52(1–192) mutant had only two thermal transitions at 47.6 and 100.9 °C (labeled B and C). Transitions were labeled such that transition C corresponds to complete unfolding of the protein. The effect of temperature and protein concentration on RAD52 self-association was analyzed by dynamic light scattering. From these data a four-state hypothetical model was developed to explain the thermal denaturation profile of wild-type RAD52. The three thermal transitions in this model were assigned as follows. Transition A was attributed to the disruption of higher order assemblies of RAD52 rings, transition B to the disruption of rings to individual subunits, and transition C to complete unfolding. The ring-shaped quaternary structure of RAD52 and the formation of higher ordered complexes of rings appear to contribute to the extreme stability of RAD52. Higher ordered complexes of rings are stable at physiological temperatures in vitro.

RAD52<sup>1</sup> protein plays a critical role in mitotic and meiotic recombination as well as double-strand break repair (1, 2). On the basis of a series of protein–protein interaction assays and DNA binding studies (3–5), a domain map of human RAD52 (RAD52) was proposed by Park et al. (Figure 1). Electron microscopy (EM) studies of *Saccharomyces cerevisiae* and human RAD52 have revealed formation of ring-shaped structures (9–13 nm in diameter), as well as higher order aggregates (6–8). The RAD52 rings appear to be composed of seven subunits (9). EM studies also showed that RAD52 recognizes and binds to double-stranded DNA ends as an aggregated complex that ranges in size from approximately 15 to 60 nm in diameter (8). This binding promoted end-to-end association between DNA molecules and stimulated the ligation of both cohesive and blunt DNA ends (8). Recently, by studying wild type and two deletion mutants of RAD52 (Figure 1), we demonstrated that the self-association domain in the N-terminal half of RAD52 is responsible for ring formation and that elements in the C-terminal half of the molecule participate in the formation of higher order complexes of rings (10).

Due to the biological interest of human RAD52 and the apparent biochemical importance of RAD52 self-association in DNA repair, we studied its multiple levels of self-association and stability using biophysical methods. The stability of wild-type RAD52 was studied by differential scanning calorimetry (DSC). To investigate the basis for the extreme stability of RAD52 that was discovered, two mutants were also studied, RAD52(1–192) and RAD52(218–418) (Figure 1). The effects of temperature and protein concentration on the hydrodynamic radius ( $R_H$ ) of RAD52 were studied by dynamic light scattering (DLS). Finally, a hypothetical model of the effects of protein aggregation state on thermal stability was developed.

## MATERIALS AND METHODS

**Protein Purification.** The domain structures for wild-type RAD52, RAD52(1–192), and RAD52(218–418) are described in Figure 1. Proteins were expressed, purified under reducing conditions, and concentrated as described (10). Unfortunately, enterokinase cleavage was nonspecific, and the histidine-patch thioredoxin (Invitrogen) could not be separated from the 218–418 peptide (Jackson, unpublished results). After the extreme thermal stability of wild-type RAD52 was observed, subsequent purifications included a heat treatment step. The lysate was heated to 55 °C for 30 min prior to the chromatography steps. Samples were concentrated using an Ultrafree-15 centrifugal filter device. After each step of concentration, the samples were analyzed by DLS. Protein concentrations were determined using the Bradford assay (Bio-Rad) with bovine serum albumin as a standard.

<sup>†</sup> This work was supported by the U.S. Army Medical Research and Material Command under DAMD17-98-1-8251 (G.E.O.B.), DAMD17-00-1-0469 (W.R.), and DAMD17-00-1-0467 (D.J.).

\* To whom correspondence should be addressed. Telephone: 419-530-1501. Fax: 419-530-4033. E-mail: gborgst@uoft02.utoledo.edu.

<sup>1</sup> Abbreviations: RAD52, human RAD52; DLS, dynamic light scattering; DSC, differential scanning calorimetry; EM, electron microscopy; MnSOD, manganese superoxide dismutase; SOS, sum of squares;  $R_H$ , hydrodynamic radius;  $T_m$ , melting temperature.

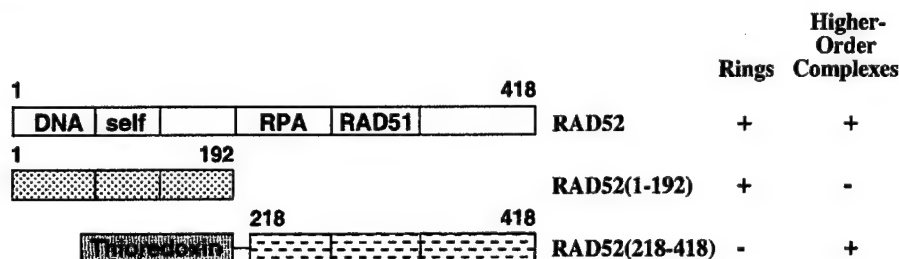


FIGURE 1: Wild-type RAD52 and deletion mutants. Beginning and ending residue numbers of each mutant are indicated along with domain structure. The following domains and residue numbers were defined by Park et al. (16): DNA binding (39–80), self-association (85–159), RPA binding (221–280), and RAD51 binding (290–330). The structural characterization of wild-type and mutant RAD52 by Ranatunga et al. is summarized on the right (10). Wild-type RAD52 and RAD52(1–192) have six histidines fused to the C-terminus. For the RAD52(218–418) mutant, a thrombin-cleavable six-histidine tag is fused to the N-terminus of the histidine-patch thioredoxin, and an enterokinase cleavage site separates histidine-patch thioredoxin from RAD52(218–418).

**Differential Scanning Calorimetry.** Protein and reference solutions were degassed under a vacuum for 15 min before data acquisition. The concentration of wild-type RAD52 was 2.0 and 3.5 mg/mL, RAD52(1–192) was 7.2 mg/mL, and RAD52(218–418) was 3.1 mg/mL. The wild-type RAD52 sample was concentrated to 11.5 mg/mL before dilution to either 2.0 or 3.5 mg/mL. The concentrations of wild-type RAD52 and RAD52(218–418) were limited by the quantity of protein available. The protein samples and reference solutions were loaded into their respective cells in the MicroCal MC-2 differential scanning calorimeter. An external pressure of 30 psi was applied with nitrogen gas to both sample and reference cells. The sample was scanned relative to the reference solution over a temperature range of 5–120 °C at a rate of 45 °C/h. DSC measurements on buffer alone had no transitions for the temperature range 5–120 °C. The baseline and change in specific heat ( $\Delta C_p$ ) upon denaturation were corrected according to standard techniques (11). DSC data were fit to a two- or three-state model using the Origin DSC software provided by Microcal Inc.

**Dynamic Light Scattering Analysis.** DLS was carried out using a DynaPro-801 molecular sizing instrument equipped with a temperature-controlled micro-sampler (Protein Solutions). A 50  $\mu$ L sample was passed through a filtering assembly equipped with a 100 nm filter into a 12  $\mu$ L chamber quartz cuvette. For each experiment, 35–60 measurements were taken. The data were first analyzed using Dynamics 4.0 software and then with DynaLS software. The refractive index and viscosity of the buffer at each temperature were measured and the proper corrections applied to the data. Baseline and sum of squares (SOS) error values were reported by Dynamics 4.0. The baseline is the measured value of the last coefficient in the correlation curve. Baselines within the range from 0.977 to 1.002 were interpreted as monomodal, and those greater than 1.002 were bi- or multimodal. The SOS error is the sum of squares difference between the measured correlation curve and the best-fit curve. SOS errors less than 5.000 were considered negligible. Errors between 5.000 and 20.000 were considered as low and probably due to low protein concentration or a small amount of polydispersity. Errors greater than 20.000 were considered as high and are probably due to high polydispersity in size distribution (aggregation) or irregular solvent. Mean  $R_H$ , standard deviation, and percent of peak area are reported from DynaLS using the optimized resolution. Due to the irregular solvent, the SOS errors increased for diluted

samples, and it was necessary to use DynaLS to separate the solvent peak from the protein peak.

## RESULTS AND DISCUSSION

**Differential Scanning Calorimetry.** Thermal stability profiles of wild-type RAD52, RAD52(1–192), and RAD52(218–418) were obtained by DSC (Figure 2 and Table 1). For wild-type RAD52 and RAD52(1–192) the DSC transitions were labeled A, B, or C such that total unfolding was always labeled C. For wild-type RAD52, at 2.0 mg/mL, the DSC profile was composed of two transitions (labeled B and C) with melting temperatures ( $T_M$ ) of 78.3 and 101.6 °C (Table 1). At 3.5 mg/mL, the wild-type RAD52 DSC profile was composed of three distinct transitions (labeled A, B, and C in Figure 2A) with  $T_M$ 's of 38.8, 73.1, and 115.2 °C (Table 1). When the concentration of wild-type RAD52 was increased, transition C was shifted to a higher temperature by 13 °C. Transition A could be measured only if the sample was first concentrated to 11.5 mg/mL and then diluted to 3.5 mg/mL. For RAD52(1–192) two transitions were observed at 47.6 and 100.9 °C (labeled B and C in Figure 2B). The deletion of the C-terminal half of RAD52 decreased the  $T_M$  of transitions B and C by 25 and 14 °C, respectively.

Our earlier analysis demonstrated that wild-type RAD52 forms ring structures as well as higher order complexes of rings but RAD52(1–192) forms rings but not the aggregates of rings (10). The size of the wild-type RAD52 higher order complexes, as well as the proportion of the rings in a higher order complex, is dependent on concentration. RAD52(1–192) rings do not form higher ordered complexes, at any concentration. DSC transition A was dependent on the concentration of wild-type RAD52 and was not observed for RAD52(1–192). Therefore, it appeared that transition A corresponded to the thermal disruption of aggregates to form single rings in solution, transition B to the break up of rings to monomers, and transition C to the total unfolding of monomers.

The DSC profile of RAD52(218–418) is also consistent with this interpretation (Figure 2C). RAD52(218–418) forms a complex of two to four monomers depending on the concentration but does not form ring structures in solution (10). It has a relatively low  $T_M$  of 53–59 °C, and it appears that the C-terminal half of RAD52, which cannot form rings, is not as thermally stable as the ring-structured N-terminal half.

Wild-type *Escherichia coli* thioredoxin is a very stable protein with a  $T_M$  of ~85 °C for the oxidized form and ~73

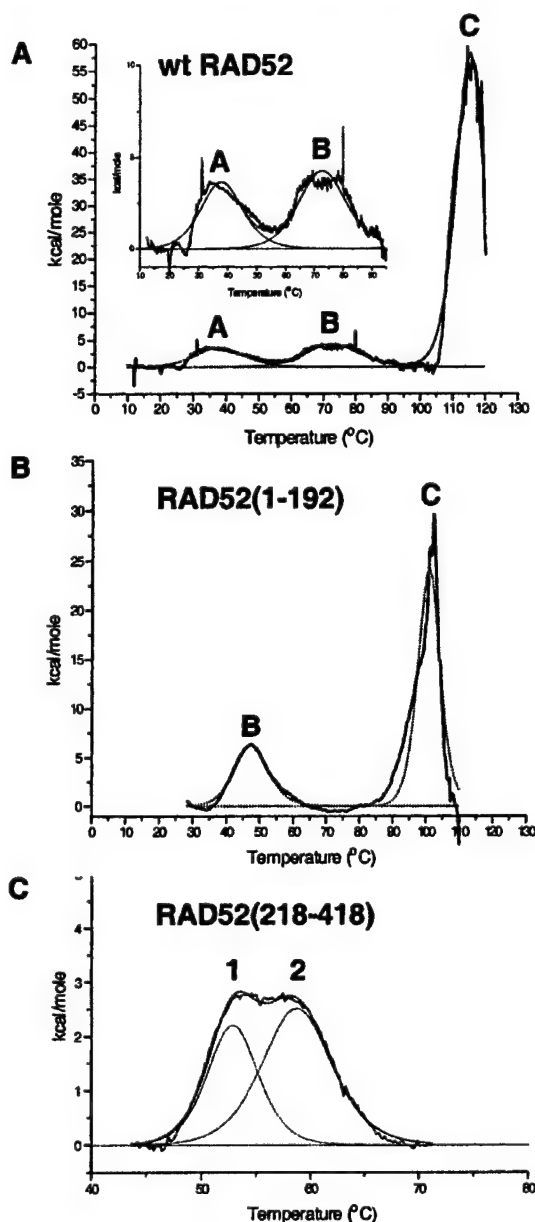


FIGURE 2: Thermal stability of wild-type RAD52 and deletion mutants. DSC profiles for (A) wild-type RAD52 were analyzed at 0.038 mM (3.5 mg/mL), (B) RAD52(1-192) at 0.325 mM (7.2 mg/mL), and (C) RAD52(218-418) at 0.082 mM (3.1 mg/mL). For RAD52(218-418) there were no transitions above 70 °C.

°C for the reduced form (12, 13). When thioredoxin is fused to other proteins, it can improve their solubility and, especially when in the oxidized form, improve their thermal stability, allowing a heat step during purification. Histidine-patch thioredoxin in the reduced state was expected to have a  $T_M$  of ~67 °C (12-14). We were unable to specifically cleave thioredoxin from RAD52(218-418) with enterokinase, so the exact contributions of thioredoxin and RAD52(218-418) to the DSC profile of the fusion protein could not be determined. It is apparent that fusing thioredoxin to RAD52(218-418) has reduced the  $T_M$  of thioredoxin significantly and that RAD52(218-418) by itself would prob-

Table 1: Thermodynamic Parameters from DSC Measurement of RAD52 Proteins

protein	concn (mg/mL)	component	$T_M$ (°C)
RAD52 <sup>a</sup>	2.0	B	78.3
		C	101.6
RAD52 <sup>b</sup>	3.5	A	38.8
		B	73.1
		C	115.2
RAD52(1-192) <sup>c</sup>	7.2	B	47.6
		C	100.9
RAD52(218-418) <sup>d</sup>	3.1	1	53.4
		2	59.1

<sup>a</sup> This sample was concentrated to 11.5 mg/mL and then diluted to 2.0 mg/mL (similar to Table 2, line 12) and does not contain higher ordered assemblies of rings. <sup>b</sup> This sample was concentrated to 11.5 mg/mL and then diluted to 3.5 mg/mL for DSC measurements (similar to Table 2, line 7, and Figure 3E) and contains higher ordered complexes of rings. <sup>c</sup> RAD52(1-192) forms rings but does not form higher ordered assemblies of rings (10). <sup>d</sup> RAD52(218-418) does not form rings but does self-associate (10).

ably have a  $T_M$  lower than that measured for the fusion protein.

The reversibility of transitions A, B, and C for wild-type RAD52 was studied by DSC, using an 11.5 mg/mL sample diluted to 3.5 mg/mL. Three experiments were performed, and the presence of precipitation was noted after each (data not shown). First, the sample was heated to 55 °C and then slowly returned to 20 °C overnight. Transition A was observed, and the protein remained in solution. Then the same sample was heated to 95 °C and slowly returned to 20 °C overnight. During this second experiment, transition A did not return, possibly due to the protein concentration used (see discussion of DLS data, Table 2, lines 7-9), and transition B was lowered to 65 °C. After the second experiment there was a slight amount of precipitate, but the majority of the protein was still in solution. For the third experiment, the sample was heated to 120 °C, and there was only one significant peak at 94 °C and the protein completely precipitated. The  $T_M$  for complete unfolding was lower than that measured from fresh sample (115 °C for peak C, Figure 2A), indicating that the protein did not properly reassemble after the second experiment and that the process of unfolding is irreversible under this set of experimental conditions.

The irreversibility of transition B was also noted in experiments performed during the addition of a heat step to the purification protocol for wild-type RAD52. Lysates were heated in 5 deg increments between 55 and 80 °C, centrifuged, and analyzed by SDS-PAGE. RAD52 began to precipitate after 65 °C (data not shown). This supports the conclusion that transition B in the thermal denaturation of RAD52 is irreversible.

**Dynamic Light Scattering.** The response of RAD52 rings and higher ordered complexes to concentration and temperature was studied by DLS. The upper temperature limit of the DLS microscopier was 50 °C so theoretically data on transition A of wild-type RAD52 and transition B of RAD52(1-192) could be measured.

The procedure followed for sample preparation affected the detection of DSC transition A and the  $T_M$  value of transition C for wild-type RAD52, so the effects of protein concentration and temperature on the  $R_H$  of wild-type RAD52 were studied using DLS. In a series of experiments, the protein concentration was increased from 3.5 to 11.5 mg/

Table 2: Effect of Temperature and Concentration on  $R_H$  of Wild-Type RAD52

DLS expt	concn (mg/mL)	base-line	SOS error <sup>a</sup>	$R_H^b$ (nm)	peak area <sup>c</sup> (%)	interpretation <sup>d</sup>
1. 20 °C	3.5	1.001	4.22	<b>15.0 (2.5)</b>	<b>98.3</b>	>2 rings
2. heat to 50 °C	3.5	1.000	2.78	<b>14.2 (4.5)</b>	<b>99.2</b>	~2 rings
3. concd; 20 °C	4.9	1.002	2.03	4.3 (0.5)	3.4	monomer
				<b>18.7 (2.3)</b>	<b>95.8</b>	>2 rings
4. concd; 20 °C	11.5	1.009	7.78	5.1 (0.6)	4.2	mono/dimer
				<b>17.8 (3.1)</b>	<b>56.9</b>	>2 rings
				<b>36.1 (4.4)</b>	<b>36.6</b>	>2 rings
5. heat to 50 °C	11.5	1.000	5.96	<b>19.2 (8.5)</b>	<b>99.2</b>	>2 rings
6. cool to 20 °C	11.5	1.010	8.24	5.9 (0.4)	9.7	mono/dimer
				11.2 (0.7)	6.6	1–2 rings
				<b>20.6 (2.2)</b>	<b>81.6</b>	>2 rings
7. sample from line 4 diluted; 20 °C	3.5	1.001	11.3	3.8 (0.2)	0.6	monomer
				<b>23.2 (11.6)</b>	<b>98.1</b>	>2 rings
8. heat to 50 °C	3.5	1.001	9.41	<b>9.7 (1.2)</b>	<b>45.8</b>	1 ring
				<b>17.0 (1.0)</b>	<b>49.8</b>	>2 rings
9. cool to 20 °C	3.5	1.001	16.1	3.9 (0.2)	1.1	monomer
				<b>11.9 (1.9)</b>	<b>69.3</b>	1–2 rings
				<b>28.6 (3.5)</b>	<b>26.4</b>	>2 rings
10. sample from line 3 diluted; 20 °C	3.3	1.001	7.4	3.1 (0.2)	11.0	monomer
				<b>16.8 (5.4)</b>	<b>84.0</b>	>2 rings
11. heat to 37 °C	3.3	1.000	7.9	<b>49.5 (8.7)</b>	<b>14.5</b>	>2 rings
12. sample from line 4 diluted; 20 °C	2.3	1.001	50.9	<b>8.75 (6.0)</b>	<b>79.7</b>	1 ring
13. heat to 37 °C	2.3	1.000	24.5	<b>8.0 (1.6)</b>	<b>71.9</b>	1 ring
14. heat to 50 °C	2.3	1.000	15.9	<b>8.7 (2.7)</b>	<b>87.4</b>	1 ring

<sup>a</sup> SOS = sum of squares. <sup>b</sup> Average  $R_H$  is given with the standard deviation given in parentheses. <sup>c</sup> DynaLS results; the percent peak area for the solvent peaks was not reported. DLS measurements at 20 and 50 °C on solvent alone indicate that very small and very large components in the RAD52 measurements were due to the solvent and not the protein. Therefore, only the peaks attributable to RAD52 protein are reported ( $R_H > 3.0$  nm; see Figure 4).  $R_H$  and percent peak area of the primary species in solution (greater than 10%) are in bold. <sup>d</sup> Interpretation is based on estimated  $R_H$  in Figure 4. It is not possible to tell exactly how many rings of RAD52 are in the aggregates >14.1 nm since the structure of the higher order complexes of RAD52 rings is unknown.

mL and then diluted (see Table 2 and Figure 3). The micro-sampler cell was held at 20, 37, or 50 °C, and samples were equilibrated for 30 min at the target temperature before DLS measurements began. The smallest  $R_H$  measured for RAD52 was 8.0–8.75 nm (Table 2, lines 12–14). This is close to the size expected for single rings measured from electron micrographs (Figure 4) (6–8). A monomer of RAD52 is expected to have an  $R_H$  value of 3.2 nm, and complexes containing two rings are expected to have an  $R_H$  of 12.8–14.1 nm. The  $R_H$  for aggregates of more than two rings would be greater than 14 nm.

Using these estimates of particle sizes as a guide, four trends in the DLS data were noted. First, heating the protein samples from 20 to 50 °C caused the  $R_H$  to decrease in general, and frequently the baseline decreased to within the monomodal range. For example, heating a sample similar to that used for DSC measurements (Table 2, line 7, and Figure 3E) caused the particles to shift from a single population with  $R_H$  of 23.2 nm to two populations with  $R_H$  of 9.7 and 17.0 nm (Table 2, line 8, and Figure 3F). Second, the size of the sample population was dependent on the protein concentration. For example, the  $R_H$  of the sample

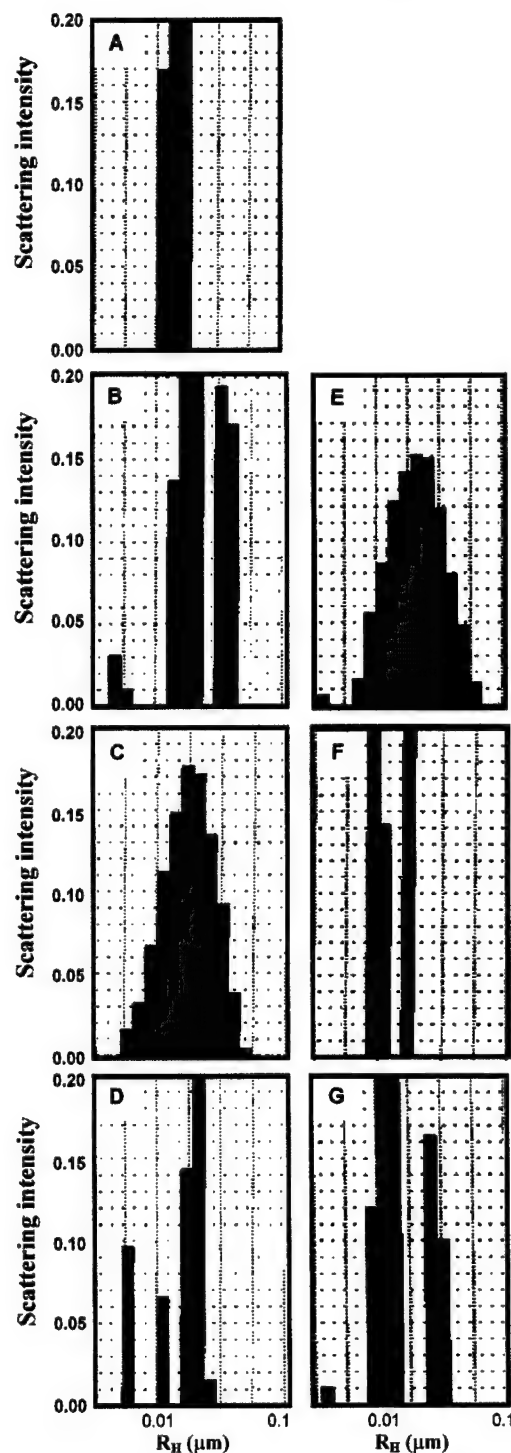


FIGURE 3: Effect of protein concentration and temperature on the  $R_H$  of wild-type RAD52. DLS data were analyzed using DynaLS software. The data correspond to the following lines in Table 2: (A) 3.5 mg/mL at 20 °C (line 1), (B) 11.5 mg/mL at 20 °C (line 4), (C) 11.5 mg/mL at 50 °C (line 5), (D) 11.5 mg/mL cooled to 20 °C (line 6), (E) diluted to 3.5 mg/mL at 20 °C (line 7), (F) diluted to 3.5 mg/mL at 50 °C (line 8), and (G) diluted to 3.5 mg/mL cooled to 20 °C (line 9). Panels E–G correspond to the sample used for DSC.



Model	$R_H$ (nm)
Monomer	3.2
7-membered ring	8.5
Two edge on rings	14.1
Two stacked rings	12.8

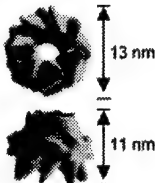


FIGURE 4: Estimated  $R_H$  for RAD52 models. The  $R_H$  for a monomer was calculated from a molecular mass of 47.0 kDa with the molecular weight calculator included in the Dynamics 3.0 software.  $R_H$  for a seven-membered ring of RAD52 was estimated from the diagonal of the three-dimensional reconstruction on the basis of electron micrographs (9). Electron micrographs of RAD52 rings in the large, greater than 100 nm spherical aggregates appear to have an "edge-on" orientation (10). The three-dimensional reconstructions of RAD52 were adapted from Stasiak et al. (2000).

population increased from 15.0 to 18.7 to 36.1 nm, when the concentration was increased from 3.5 to 4.9 to 11.5 mg/mL (Table 2, lines 1, 3, and 4). Third, the modality of the sample population was dependent on the protein concentration. For example, the 11.5 mg/mL sample was multimodal at 20 °C (Table 2, line 4, and Figure 3B), and the 3.5 mg/mL sample was not (Table 2, line 1, and Figure 3A). Fourth, the reversibility of the assembly of RAD52 rings into higher ordered complexes was dependent on protein concentration. The majority of the particles in the samples at 11.5 mg/mL remained greater than 17 nm throughout the heat cycle (Table 2, lines 4–6, and Figure 3B–D). But, the superaggregation of rings was only partially reversible at 3.5 mg/mL with only 26% of the sample returning to greater than 17 nm after being heated (Table 2, lines 7–9, and Figure 3E–G). It is noteworthy that for the DSC measurements made on samples at 3.5 mg/mL the assembly of RAD52 rings into higher ordered complexes is not completely reversible at this concentration.

Finally, this DLS analysis facilitated the interpretation of DSC transition A. Transition A could not be detected for samples that were first concentrated to 11.5 mg/mL and then diluted to 2.0 mg/mL (prepared as in line 12, Table 2). The  $R_H$  value of 8.75 indicates that at 2.0 mg/mL there are primarily single rings in solution and little or no higher ordered complexes (Figure 4). Transition A was detectable for samples that were diluted to 3.5 mg/mL (prepared as in line 7, Table 2, and Figure 3E). The  $R_H$  value of 23.2 nm indicates that at 3.5 mg/mL there are primarily higher order complexes of many rings in solution. Heating this sample to 50 °C caused the  $R_H$  to decrease and form two populations of 9.7–17.0 nm (Table 2, line 8, and Figure 3F). Therefore, these DLS data indicate that DSC transition A can be attributed to the disassociation of rings from higher ordered complexes.

We were interested to know if the higher ordered complexes of RAD52 rings were stable at physiological temperatures. Protein samples diluted to 3.3 mg/mL did not form particles less than 9 nm upon heating to 37 °C (Table 2, lines 10 and 11) although the samples became monomodal. Therefore, the upper level aggregation of RAD52 rings is stable at physiological temperatures *in vitro*.

Transition B of the RAD52(1–192) mutant was 47.6 °C, and attempts were made to measure the effect of temperature on the structure of RAD52(1–192) with DLS. Higher ordered assemblies of rings are not formed by RAD52(1–

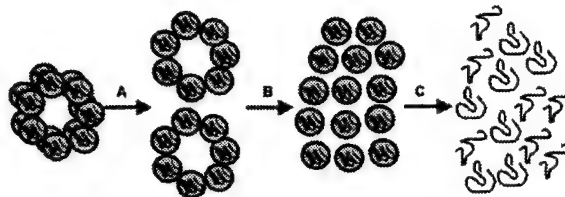


FIGURE 5: Hypothetical four-state model for the thermal denaturation of wild-type RAD52. Transitions A, B, and C correspond to those measured by DSC in Figure 2. There are three transitions in this model; transition A is attributed to the disruption of higher order assemblies of RAD52 rings, transition B to the disruption of rings to individual subunits, and transition C to complete unfolding. The individual subunits after transition B are probably partially unfolded as well as disassociated from the rings.

192), and single rings have an  $R_H$  of 5.7 nm (SD = 1.2) (10). As samples of RAD52(1–192) were heated, the  $R_H$  appeared to increase, perhaps indicating partial unfolding (data not shown). DLS measurements at elevated temperatures with RAD52(1–192) were very problematic, and at 50 °C no measurements could be obtained, perhaps due to large changes in structure.

## CONCLUSIONS

Our data indicate that the RAD52 rings and higher ordered complexes of rings used in DNA repair and DNA recombination are extremely stable structures. The structure of wild-type RAD52 is very stable, and its multiple levels of self-association appear to contribute to this stabilization. The extreme stability of the wild-type RAD52 and RAD52(1–192) folds relative to RAD52(218–418) appears to be related to the assembly of multiple monomers into a ring. The enhanced stability of the wild-type RAD52 fold relative to RAD52(1–192) appears to be due in part to its ability to form higher order assemblies of rings.

A four-state hypothetical model has been developed to explain the thermal denaturation profile of wild-type RAD52 (Figure 5). There are three transitions in this model; transition A is attributed to the disruption of higher order assemblies of RAD52 rings, transition B to the disruption of rings to individual subunits, and transition C to complete unfolding. Individual rings of RAD52 appear to have an  $R_H$  on the order of 8.0–8.75 nm in solution (Table 2, lines 12–14). Higher order assemblies of rings are seen in the wild-type RAD52 DLS data as particles ranging from 15 to 50 nm. Note that the measured  $R_H$  values are not integral values of individual rings due to the presence of equilibrium mixtures of single rings and complexes of rings in solution as indicated by the high standard deviations in the  $R_H$  measurements (Table 2) and the width of the DLS peaks (Figure 3). This equilibrium is dependent upon concentration. At concentrations of 3.5 mg/mL or greater RAD52 appears to be primarily composed of assemblies of two or more rings with  $R_H$  values ranging from 15 to 36.1 nm. Raising the temperature from 20 to 50 °C disrupts the higher order particles, pushing the equilibrium toward the 9 nm particles (Table 2, lines 5 and 8, and Figure 3C and F). These data support our hypothetical model for transition A (Figure 5). Reliable DLS measurements varying temperature on RAD52(1–192) could not be made. Thermal expansion of the RAD52(1–192) rings was noted. The data indicate that a large structural transition occurs near transition

B, possibly the disassociation of individual subunits from the rings.

Only a handful of proteins have been measured with thermal stabilities on the order of RAD52. To our knowledge, the highest  $T_M$  for a protein reported in the literature to date is 125 °C for ferredoxin from the hyperthermophile *Thermotoga maritima* (15). Other proteins such as onconase and mitochondrial manganese superoxide dismutase (MnSOD) are extremely stable with  $T_M$ 's approaching 90 °C (16, 17). Both ferredoxin and onconase are monomeric, and by studying their protein crystal structures, their stabilities were attributed to the compactness of their tertiary structures and to extensive hydrogen bonding involving charged amino acid side chains. Mitochondrial MnSOD is a homotetramer, and its enhanced stability was partially attributed to its quaternary structure. The DSC profile of MnSOD has three thermal transitions (labeled A, B, and C), similar to those seen with RAD52. Transition A was attributed to subunit disassociation, transition B to loss of the active site manganese, and transition C to complete unfolding. A cavity forming point mutation in the tetrameric interface of MnSOD resulted in the lowering of transition B by 13.6 °C and transition C by 16.5 °C (17). These results on MnSOD are somewhat similar to the results on RAD52. We conclude from our data that both components of RAD52 self-association, ring formation and higher order complex formation, contribute to its extreme thermal stability. A precise understanding of the structural determinants of RAD52 stability awaits the solution of its crystal structure.

#### ACKNOWLEDGMENT

We thank Dr. Min Park for providing the expression plasmid for RAD52(1–192).

#### REFERENCES

- Game, J., and Mortimer, R. K. (1974) *Mutat. Res.* 24, 281–292.
- Petes, T. D., Malone, R. E., and Symington, L. S. (1991) in *The Molecular and Cellular Biology of the Yeast, Saccharomyces* (Broach, J. R., Pringle, J. R., and Jones, E. W., Eds.) pp 407–522, Cold Spring Harbor Laboratory Press, Cold Spring Harbor, NY.
- Shen, Z., Cloud, K. G., Chen, D. J., and Park, M. S. (1996) *J. Biol. Chem.* 271, 148–152.
- Shen, Z., Peterson, S. R., Comeaux, J. C., Zastrow, D., Moyzis, R. K., Bradbury, E. M., and Chen, D. J. (1996) *Mutat. Res.* 364, 81–89.
- Park, M. S., Ludwig, D. L., Stigger, E., and Lee, S. H. (1996) *J. Biol. Chem.* 271, 18996–19000.
- Shinohara, A., Shinohara, M., Ohta, T., Matsuda, S., and Ogawa, T. (1998) *Genes Cells* 3, 145–156.
- Van Dyck, E., Hajibagheri, N. M. A., Stasiak, A., and West, S. C. (1998) *J. Mol. Biol.* 284, 1027–1038.
- Van Dyck, E., Stasiak, A. Z., Stasiak, A., and West, S. C. (1999) *Nature* 398, 728–731.
- Stasiak, A. Z., Larquet, E., Stasiak, A., Muller, S., Engel, A., Dyck, E. V., West, S. C., and Egelman, E. H. (2000) *Curr. Biol.* 10, 337–340.
- Ranatunga, W., Jackson, D., Lloyd, J. A., Forget, A. L., Knight, K. L., and Borgstahl, G. E. O. (2001) *J. Biol. Chem.* (in press).
- Haynie, D. T., and Freire, E. (1994) *Anal. Biochem.* 216, 33–41.
- Ladbury, J., Wynn, R., Hellinga, H., and Sturtevant, J. (1993) *Biochemistry* 32, 7526–7530.
- Ladbury, J., Kishore, N., Hellinga, H., Wynn, R., and Sturtevant, J. (1994) *Biochemistry* 33, 3688–3692.
- Lu, Z., DiBlasio-Smith, E., Grant, K., Warne, N., LaVallie, E., Collins-Racie, L., Follettie, M., Williamson, M., and McCoy, J. (1996) *J. Biol. Chem.* 271, 5059–5065.
- Pfeil, W., Gesierich, U., Kleemann, G. R., and Sterner, R. (1997) *J. Mol. Biol.* 272, 591–596.
- Notomista, E., Catanzano, F., Graziano, G., Piaz, F. D., Barone, G., D'Alessio, G., and Donato, A. D. (2000) *Biochemistry* 39, 8711–8718.
- Borgstahl, G. E. O., Parge, H. E., Hickey, M. J., Johnson, M. J., Boissinot, M., Hallewell, R. A., Lepock, J. R., Cabelli, D. E., and Tainer, J. A. (1996) *Biochemistry* 35, 4287–4297.

BI0155089

**JMB**

## Analysis of the Human Replication Protein A:Rad52 Complex: Evidence for Crosstalk Between RPA32, RPA70, Rad52 and DNA

Doba Jackson<sup>1</sup>, Kajari Dhar<sup>2</sup>, James K. Wahl<sup>3</sup>, Marc S. Wold<sup>2</sup> and Gloria E. O. Borgstahl<sup>1\*</sup>

<sup>1</sup>Department of Chemistry  
University of Toledo  
2801 West Bancroft Street  
Toledo, OH 43606-3390, USA

<sup>2</sup>Department of Biochemistry  
University of Iowa College of  
Medicine, 51 Newton Road  
Iowa City, IA 52242-1109  
USA

<sup>3</sup>Department of Biology  
University of Toledo, Toledo  
OH 43606-3390, USA

The eukaryotic single-stranded DNA-binding protein, replication protein A (RPA), is essential for DNA replication, and plays important roles in DNA repair and DNA recombination. Rad52 and RPA, along with other members of the Rad52 epistasis group of genes, repair double-stranded DNA breaks (DSBs). Two repair pathways involve RPA and Rad52, homologous recombination and single-strand annealing. Two binding sites for Rad52 have been identified on RPA. They include the previously identified C-terminal domain (CTD) of RPA32 (residues 224–271) and the newly identified domain containing residues 169–326 of RPA70. A region on Rad52, which includes residues 218–303, binds RPA70 as well as RPA32. The N-terminal region of RPA32 does not appear to play a role in the formation of the RPA:Rad52 complex. It appears that the RPA32CTD can substitute for RPA70 in binding Rad52. Sequence homology between RPA32 and RPA70 was used to identify a putative Rad52-binding site on RPA70 that is located near DNA-binding domains A and B. Rad52 binding to RPA increases ssDNA affinity significantly. Mutations in DBD-D on RPA32 show that this domain is primarily responsible for the ssDNA binding enhancement. RPA binding to Rad52 inhibits the higher-order self-association of Rad52 rings. Implications for these results for the “hand-off” mechanism between protein–protein partners, including Rad51, in homologous recombination and single-strand annealing are discussed.

© 2002 Elsevier Science Ltd. All rights reserved

**Keywords:** human Rad52; replication protein A; double-strand break repair; protein–protein interaction; single-stranded DNA binding

\*Corresponding author

### Introduction

The repair of double-strand breaks (DSBs) in chromosomal DNA is of critical importance for

the maintenance of genomic integrity. In *Saccharomyces cerevisiae*, genes of the RAD52 epistasis group were identified initially by the sensitivity of mutants to ionizing radiation.<sup>1</sup> These genes have been implicated in an array of recombination events, including mitotic and meiotic recombination as well as DSB repair. The importance of specific protein–protein interactions in the catalysis of homologous recombination is suggested by studies that demonstrate specific contacts and functional interactions between scRad52, scRPA and scRad51.<sup>2–6</sup> Studies of the equivalent human proteins have identified similar interactions.<sup>7–9</sup>

Rad52 protein plays a critical role in mitotic and meiotic recombination as well as DSB repair.<sup>1</sup> On the basis of a series of protein–protein interaction assays and DNA-binding studies, a domain map of human Rad52 was proposed (shown in Figure 1).<sup>10</sup>

Abbreviations used:  $C_p$ , polydispersity; CTD, C-terminal domain; DBD, DNA-binding domain; DLS, dynamic light-scattering; DSB, double-strand break; EM, electron microscopy; GMSA, gel mobility-shift assay; mAb, mouse monoclonal antibody; OB-fold, oligonucleotide/oligosaccharide binding; Rad52, human Rad52 protein;  $R_h$ , hydrodynamic radius; RPA, human replication protein A; RPA14, 14 kDa subunit of RPA; RPA32, 32 kDa subunit of RPA; RPA70, 70 kDa subunit of RPA; scRad52, *Saccharomyces cerevisiae* Rad52; scRPA, *Saccharomyces cerevisiae* RPA; SLS, static light-scattering; SOS, sum of squares; SPR, surface plasmon resonance; ssDNA, single-stranded DNA.

E-mail address of the corresponding author:  
[gorgst@uoft02.utoledo.edu](mailto:gorgst@uoft02.utoledo.edu)



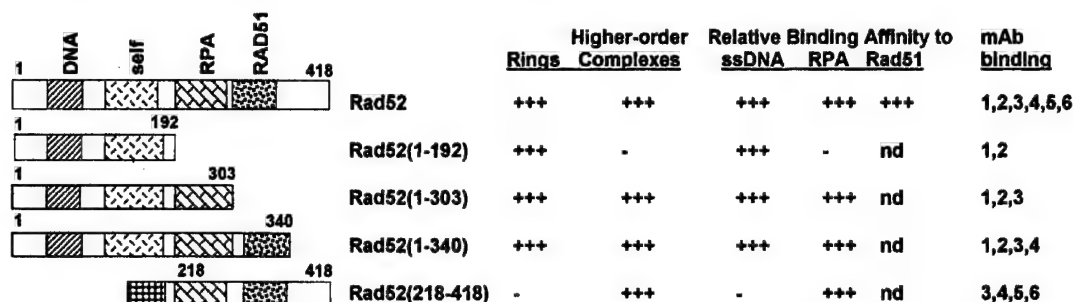


**Figure 1.** A diagram of the Rad52 domain structure, Rad52 mutants used and characterization of monoclonal antibodies developed against Rad52. Rad52 interaction domains with the residue numbers in parentheses were defined as follows: DNA-binding domain (residues 25–65), Rad52 heptameric ring binding (125–185), RPA32 binding (220–280), Rad51-binding domain (290–340).<sup>10,14,53</sup> Wild-type and mutant Rad52 are shown to the left with domains indicated and beginning and ending residue numbers included. Wild-type Rad52, Rad52(1–192), Rad52(1–303) and Rad52(1–340) pET28 expression plasmids were a gift from Dr Min Park and have six histidine residues fused to the C-terminus. For improved solubility, the Rad52(218–418) mutant has thioredoxin fused to the N terminus. This thioredoxin was modified with six histidine residues fused to its N terminus to improve purification. Characterization of each construct for ring structure, higher-order complexes, relative binding affinity for ssDNA, RPA and Rad51, as well as monoclonal antibody binding are summarized on the right.<sup>14</sup>

Rad52 has a homologous pairing activity thought to be important in Rad51-independent DSB repair, and this activity was localized to residues 1–237.<sup>11</sup> Electron microscopy (EM) studies of *S. cerevisiae* and human Rad52 have revealed formation of ring-shaped structures (9–13 nm in diameter), as well as higher-order aggregates.<sup>4,9,12</sup> The Rad52 rings appear to be composed of seven subunits.<sup>13</sup> EM studies showed that Rad52 binds to DNA ends as an aggregated complex that ranges in size from approximately 15–60 nm in diameter.<sup>12</sup> This binding has been found to promote end-to-end association between DNA molecules and to stimulate the ligation of both cohesive and blunt DNA ends. Recently, the studies with wild-type and two deletion mutants of Rad52 have demonstrated that the self-association domain in the N-terminal half of Rad52 is responsible for ring formation and that elements in the C-terminal half of the molecule participate in the formation of higher-order complexes of rings.<sup>11,14</sup> Such higher-ordered complexes of Rad52 rings have been shown by EM to mediate single-strand annealing.<sup>15</sup>

RPA is the single-stranded DNA (ssDNA) binding protein that has been found in all eukaryotes examined.<sup>16,17</sup> It is composed of three subunits that have been named for their molecular mass as RPA70, RPA32 and RPA14 (Figure 2). All three subunits of RPA are required for function. All RPA homologs bind ssDNA with high affinity and participate in specific protein-protein interactions. RPA binds tightly to ssDNA with apparent association constants of  $10^9$ – $10^{10}$  M<sup>-1</sup> and prefers polypyrimidine sequences to polypurine sequences.<sup>18–20</sup> The major binding mode for RPA has an occluded binding site of 30 nucleotides per RPA heterotrimer.<sup>21</sup> The major ssDNA binding site is located in the middle of RPA70 and is composed of two structurally conserved oligonucleotide/oligosaccharide binding (OB) domains<sup>19,22</sup> called

DBD-A (including residues 181–290) and DBD-B (residues 300–422). To date, four additional OB-folds have been identified in RPA. The N terminus (residues 1–110; called RPA70NTD), the C terminus of RPA70 (residues 432–616; called DBD-C), the central core of RPA32 and the core of RPA14 are all composed of OB-folds.<sup>23–26</sup> RPA is known to undergo a significant conformational change upon binding DNA.<sup>19,27</sup> This conformational shift has been suggested to alter the structure of RPA in a way that facilitates phosphorylation and interactions with other proteins.<sup>27</sup>

RPA is phosphorylated during the S phase of the cell-cycle, in response to DNA damage and during apoptosis.<sup>27–29</sup> The primary phosphorylation sites are located in the N-terminal 33 amino acid residues of RPA32. This DNA damage-induced phosphorylation is coincident with cell-cycle arrest and loss of the ability of cell extracts to support DNA replication<sup>30,31</sup> and in some studies leads to disassembly of the RPA heterotrimer complex.<sup>32</sup> The RPA complex appears to contain all three subunits at sites of ongoing DNA replication.<sup>33,34</sup> These observations suggest that phosphorylation of RPA serves as a mechanism for modulating RPA activity, quaternary structure and its interactions with other proteins. RPA mutants, designed to mimic biological phosphorylation by replacing Ser or Thr with Asp, have been shown to modify the activity of RPA (Braun & M.S.W., unpublished results).

RPA has specific interactions with many proteins; such as replication proteins T antigen, DNA polymerase, and DNA primase; the tumor suppressor p53; transcription factors Gal4 and VP16; and DNA repair factors, XPA, ERCC-1/XPF nuclease, XPG, uracil DNA glycosylase, Rad52 and Rad51.<sup>10,16,17,35–38</sup> Interactions between Rad51, Rad52, and RPA stimulate homologous recombination-based DSB repair.<sup>5,7,8,39</sup> An interaction region of RPA with Rad51 was located between residues

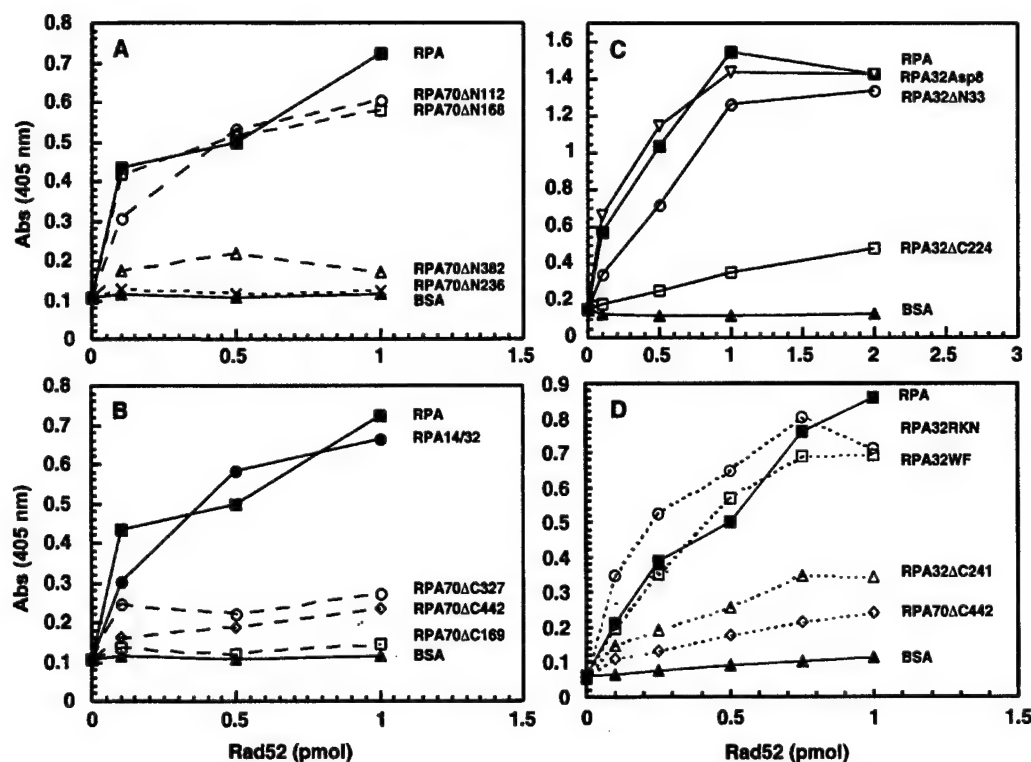
RPA70	RPA32	RPA14		Relative Binding Affinity to			SV40 DNA Replication
				ssDNA	Rad52	Rad51	
1 616	1 270	1 120	RPA	+++	+++	++	+
113 616	1 270	1 120	RPA70ΔN112	+++	+++	nd	+
169 616	1 270	1 120	RPA70ΔN168	+++	+++	++	+
237 616	1 270	1 120	RPA70ΔN236	+	-	-	-
383 616	1 270	1 120	RPA70ΔN382	-	-	nd	-
441 616			RPA70ΔC442	++	±	nd	-
326 616			RPA70ΔC327	+	±	++	-
168 616			RPA70ΔC169	+++	-	nd	-
1 616	8,11,12,13, 21,26,29,33D 270	1 120	RPA32D8	+++	+++	nd	+
1 616	81,85,88A 270	1 120	RPA32RKN	+++	+++	nd	+
1 616	107,135A 270	1 120	RPA32WF	+++	+++	nd	+
1 616	34 270	1 120	RPA32ΔN33	+++	+++	nd	+
1 616	1 240	1 120	RPA32ΔC241	+++	±	nd	+
1 616	1 223	1 120	RPA32ΔC224	+++	±	nd	+
1 616	1 270	1 120	RPA14/32	-	+++	++	-

Figure 2. Schematic of the RPA and RPA mutants used. The left portion shows diagrams of all RPA mutants used in this study. Beginning and ending amino acid residues of each mutant are indicated. The strength of the protein-protein interactions between RPA and Rad52 are indicated as follows (the data are summarized in Figure 1): (1) Strong complex forming (+++); (2) weak complex forming (±); (3) no complex forming (-). ELISA was used to determine protein-protein interactions with RPA mutants and Rad52 in this study. Only an interaction twofold above that of BSA was considered as a weak binding interaction, and the no complex forming proteins did not show a signal twofold above that of BSA even at higher concentrations (data not shown). Protein interactions with Rad51 by RPA and Rad52 mutants were determined in previous work.<sup>37</sup> ssDNA binding and SV40 DNA replication activities of the RPA mutants were determined in previous studies.<sup>20,35,42</sup> The nomenclature used for each RPA mutant is summarized below. Deletions from the N or C terminus are indicated by a RPA, (subunit of residues deleted—70,32), followed by Δ, then the terminus where the deletions occurred (N or C) and the amino acid residue number where the deletion started (for C-terminal deletions) or the last amino acid residue deleted (for N-terminal deletions). RPA32D8 has the following mutations S8D, S11D, S12D, S13D, T21D, S25D, S29D, and S33D, to mimic hyperphosphorylated RPA (Braun & M.S.W. unpublished results). RPA32RKN has the following mutations R81A, K85A, N89A in the putative ssDNA binding site of RPA32. RPA32WF has the following mutations W107A and F135A in the putative ssDNA binding site of RPA32.

168 and 236 of RPA70.<sup>37</sup> RPA14/32 also co-immunoprecipitated with Rad51 but the interaction with RPA32 was not explored further.<sup>37</sup> The interaction sites on RPA for Rad52 have not been mapped carefully. Human Rad52 was shown to interact strongly with RPA32 and weakly with RPA70.<sup>10</sup> Park and co-workers cited unpublished results that the acidic C terminus of RPA32 (including the last 33 amino acid residues) interacted with the basic patch of residues they had identified on Rad52.<sup>10</sup> Recently, a C-terminal fragment of RPA32 composed of residues 172–270 was studied by NMR, alone and in complex with peptides of UNG2, XPA and Rad52 (including residues 257–274).<sup>40</sup> Yet, the co-precipitation of RPA70 as well as RPA32 with Rad52 by Park indicated that the C terminus of RPA32 is only part of the Rad52 interaction surface. Two-hybrid and co-precipitation analysis of yeast proteins gave additional

evidence of the involvement of scRPA70 as well as scRPA32 in the interaction with scRad52.<sup>38</sup>

Since the interaction of Rad52 with RPA is important in DSB repair and the literature provides an incomplete description of the RPA surface that interacts with Rad52, the regions of RPA involved in binding Rad52 have been explored in detail. The protein-protein interactions of several mutants of RPA with Rad52 have been studied to define the role of the N or C terminus of RPA32, RPA phosphorylation and RPA70 in the RPA:Rad52 interaction. Our results reveal that the interaction of Rad52 with RPA involves two binding sites, one on RPA70 and one on RPA32. These results motivated a homology search that identified a putative Rad52-binding site near the major ssDNA-binding site of RPA70. A mixture of RPA:Rad52 has higher affinity for ssDNA than either RPA or Rad52 alone, and this increase



**Figure 3.** Deconvolution of the domains on RPA that bind Rad52. In the ELISA assay, wild-type or mutant RPA was immobilized on a microtiter plate. Increasing amounts of wild-type Rad52 were added to plates and washed. The bound Rad52 was detected with a specific monoclonal Rad52 antibody (mAb6, see Figure 1) followed by a peroxidase-coupled anti-mouse IgG antibody. Interactions were monitored by measuring ABTS absorbance at 405 nm after the addition of substrate and plotted against the amount of Rad52. (a) RPA and heterotrimeric mutants of RPA70, (b) RPA, RPA14/32 and RPA70 mutants, (c) RPA and heterotrimeric mutants of RPA32, and (d) RPA, heterotrimeric point mutants, RPA70 mutant and heterotrimeric mutant of RPA32. Multiple assays were performed and representative data are shown.

appears to be through increased affinity of RPA32 for ssDNA. Finally, by studying the size of the RPA:Rad52 complex in comparison to Rad52 and RPA alone, it was found that the interaction of RPA with Rad52 disrupts the higher-order aggregation of Rad52 rings and promotes single Rad52 rings in solution. Taken together with the similarity between Rad52 and Rad51-binding sites on RPA, these studies provide a molecular basis for Rad51 and Rad52 competition for binding to RPA. This competition between the protein-protein interaction surfaces of Rad52, Rad51 and RPA is likely to be critical for efficient DSB repair. The higher affinity of the RPA:Rad52 complex for ssDNA has implications for the mechanism of single-strand annealing.

## Results

### Identification of the regions of RPA important for binding Rad52

The association of Rad52 to RPA was studied using an ELISA method with purified Rad52,

wild-type and several mutant forms of RPA (Figure 2). For the ELISA, RPA was immobilized on a microtitre plate, excess sites were blocked with 5% milk and increasing concentrations of hRad52 were added, incubated and washed. Any Rad52 in complex with RPA or RPA mutants was then detected with a monoclonal antibody (mAb6, see Figure 1) that recognizes an epitope between residues 341 and 418 on the C terminus of Rad52. RPA heterotrimer deletion mutants in the N-terminal region of RPA70 are shown in Figure 3(a). In Figure 3(b), RPA heterotrimer was compared with the heterodimer and peptides of RPA70. In Figure 3(c) and (d), data on RPA heterotrimer mutants with deletions or mutations in RPA32 are shown in comparison to RPA heterotrimer and residues 1–441 of RPA70. The RPA mutants used here were used previously to map the regions of RPA binding to Rad51, XPA, DNA polymerase and T-antigen.<sup>35,37,41,42</sup>

Five primary conclusions were made on the basis of the ELISA data. First, Rad52 binding was reduced significantly when residues 224–271

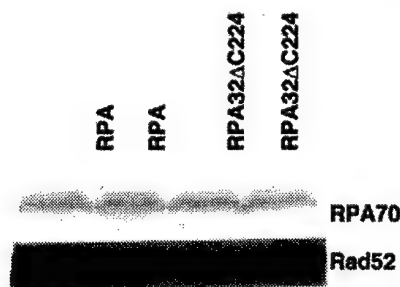


**Figure 4.** Immunoprecipitation of RPA:Rad52 and RPA32 $\Delta$ C224:Rad52 complex. Reactions (in duplicate) in lanes 1 and 2 contained wild-type RPA, and lanes 3 and 4 contained RPA32 $\Delta$ C224 as indicated. Only the data for antibody mAb3 are shown. All other antibodies gave similar results.

(Figure 3(c)) or residues 241–271 (Figure 3(d)) in the C-terminal domain (CTD) of RPA32 were deleted. This indicates a major role for the acidic C terminus of RPA32 in binding Rad52 and is consistent with previous results and predictions.<sup>10,40</sup> Second, when the N terminus of RPA32 is either deleted or mutated with changes from serine or threonine to aspartic acid (RPA32 $\Delta$ N33, RPA32Asp8, Figure 2), there is no effect on Rad52 binding. Therefore, the N terminus of RPA32, in either its neutral or acidic/hyperphosphorylated form, is probably not involved in the RPA:Rad52 interaction (Figure 3(c)). Third, Rad52 binding was destroyed when residues 169–382 were deleted from RPA70 in the trimer (Figure 3(a)). It is interesting that deletion of this region of RPA70 disrupts Rad52 binding even though intact RPA32 is present. Fourth, all RPA70 peptides (which lack RPA14/32) bind Rad52 weakly, except RPA70 $\Delta$ C169, which does not bind at all (Figure 3(b)). This result is consistent with those observed with the RPA heterotrimer mutants with N-terminal deletions in RPA70: no significant change in binding was observed when residues 1–112 or 1–168 were deleted (Figure 3(a)). Fifth, RPA14/32 binds Rad52 as tightly as the heterotrimer (Figure 3(b)), even though RPA70 is not present. In summary, these results show that the RPA:Rad52 complex is negatively affected when either residues 224–271 of RPA32 or residues 169–326 of RPA70 are missing from heterotrimeric RPA.

In immunoprecipitation reactions (Figure 4), a strong and significant interaction was seen between RPA and wild-type Rad52 and between RPA32 $\Delta$ C224 and wild-type Rad52. All six anti-Rad52 antibodies pull down both the RPA:Rad52 complex and RPA32 $\Delta$ C224 complex. The level of RPA32 $\Delta$ C224 in a complex with Rad52 relative to wild-type RPA were similar. There appear to be some differences in the binding of Rad52 to RPA32 $\Delta$ C224 in the two assays (Figures 3(c) and 4). However, it is difficult to compare the data obtained in the ELISA and immunoprecipitation reactions qualitatively, because RPA was in excess

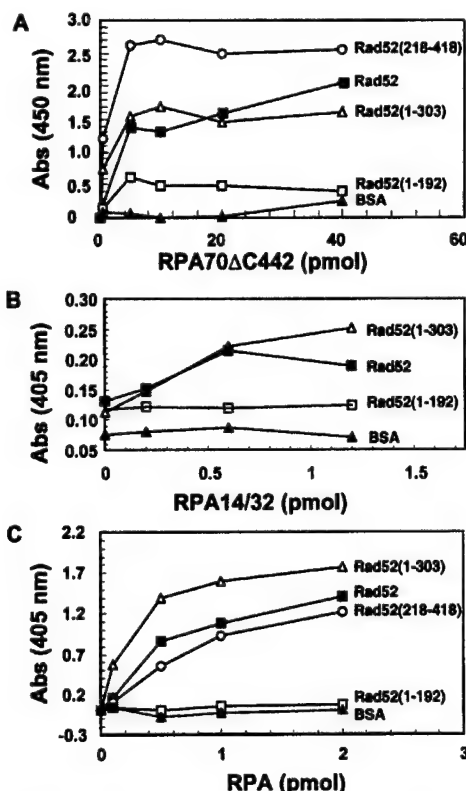


**Figure 5.** The binding of RPA70 $\Delta$ C442, RPA14/32 and wild-type RPA to Rad52. In the ELISA assay, wild-type or mutant Rad52 was immobilized on a microtiter plate. Increasing amounts of RPA were added to plates and washed. The bound Rad52 was detected with monoclonal antibodies to RPA70 or RPA32 (Calbiochem) followed by a peroxidase-coupled anti-mouse IgG antibody. Interactions were monitored by measuring TMP substrate absorbance at 450 nm or ABTS substrate at 405 nm and plotted against the amount of RPA.

in the former while Rad52 was in excess in the latter. We conclude that these studies demonstrate a strong interaction between RPA and Rad52 in solution when the RPA32CTD has been deleted, confirming a role for RPA70 in binding Rad52.

#### The region of Rad52 important for binding RPA32 and RPA70

The interaction site on Rad52 for RPA70 and RPA32 was studied using a similar ELISA protocol. Wild-type or mutant Rad52 was immobilized to a microtitre plate, excess sites were blocked with 5% milk and increasing concentrations of RPA70 $\Delta$ C442 was added, incubated and washed. Any RPA in complex with Rad52 or Rad52 mutants was then detected with a monoclonal antibody against RPA70 (Calbiochem). The data show that the primary interaction sites for both RPA70 and RPA32 are in the region including Rad52 residues

Table 1. DNA binding activity of forms of RPA, Rad52 and RPA:Rad52 complexes

GMSA data	RPA forms (ratio) <sup>b</sup>	None	$K_A (\times 10^9 \text{ M}^{-1})^a$ Rad52	Rad52(218–418)
1.	None		0.74 (0.24, V)	ND
2.	RPA (1:1)	1.4 (0.2, S)	0.75 (0.15, F)	1.3 (0.5, V)
3.	RPA (1:7)	1.4 (0.2, S)	7.5 (2.6, S)	25 (6.1, S)
4.	RPA14/32 (1:1)	ND	ND	ND
SPR data <sup>c</sup>	RPA forms (ratio) <sup>b</sup>	None	$K_A (\times 10^8 \text{ M}^{-1})^a$ Rad52	Rad52(218–418)
5.	None			ND
6.	RPA (1:7)	3.9 (0.5, S)		12 (1.7, S)
7.	RPA32RKN (1:7)	2.5 (1.3, S)		1.9 (0.5, S)
8.	RPA32WF (1:7)	2.2 (0.6, S)		2.4 (0.8, S)
9.	RPA32ΔC224 (1:7)	1.3 (0.1, V)		3.5 (0.2, S)
10.	RPA32ΔC241 (1:7)	3.1 (1.6, S)		2.4 (0.7, S)

<sup>a</sup> The error is indicated in parentheses and was estimated from the standard deviation of actual values (indicated by an S), from the variation if only two trials were done (V) or from the fitting error if the experiment was done only once (F); ND, no binding was detected.

<sup>b</sup> RPA:Rad52 complexes were mixed using the ratios indicated where the RPA component is on either the heterotrimer or heterodimer basis and the Rad52 component is on a monomer basis.

<sup>c</sup> Assay done in 1 M KCl.

193–303 (Figure 5). The Rad52(218–418), and Rad52(1–303) showed slightly higher binding activity than wild-type Rad52, perhaps due to increased exposure to the RPA-binding domain.

#### Effect of Rad52 binding on RPA ssDNA binding

The RPA70 binding site (residues 169–326) for Rad52 identified by protein–protein interaction studies includes all of ssDNA binding site DBD-A and a portion of DBD-B. Therefore, the ability of Rad52 to modulate the affinity of RPA for dT<sub>30</sub> ssDNA was studied (Table 1 and Figure 6). Using the gel mobility-shift assay (GMSA) under physiological salt concentrations, wild-type RPA had a  $K_A$  of  $1.4 \times 10^9 \text{ M}^{-1}$ , wild-type Rad52 had a  $K_A$  of  $0.74 \times 10^9 \text{ M}^{-1}$ , and no binding was detectable for the Rad52(218–418) mutant (Table 1, rows 1–3; see also Figure 6(a)). Surprisingly, the affinity of the RPA:Rad52 complexes for ssDNA was fivefold to 18-fold higher than RPA or Rad52 alone (Table 1, row 3). The stimulatory effect of the Rad52(218–418) mutant is particularly significant, since this mutant retains the full RPA binding surface but has no detectable affinity for DNA (Table 1, row 3; see also Figure 6(a)).

The effect of the molar ratio of Rad52 monomer to RPA heterotrimer on ssDNA binding affinity of the RPA:Rad52 complexes was studied using GMSA (Table 1 and Figure 6(b)). For wild-type proteins, the 1 to 7 ratio gave maximal binding and the 1 to 14 ratio gave similar binding (Figure 6(b)). Wild-type Rad52 was assumed to be in a heptameric ring. For the RPA:Rad52(218–418) complex, the stoichiometry of binding for the protein–protein complex was not known, so a series of ratios were tested for ssDNA affinity. DNA affinity increased as the ratio increased and was maximal at the 1 to 7 ratio (Figure 6(b)). With

both Rad52 and Rad52(218–418), no stimulation was observed at a 1:1 molar ratio (Table 1, line 2). This suggests that this ratio is too low for a stimulatory interaction or complex to form. Fivefold to 18-fold stimulation was observed at a 1:7 molar ratio (Table 1, row 3). This stimulation was probably not caused by non-specific protein effects, because all reactions contained 50  $\mu\text{g}/\text{ml}$  of bovine serum albumin (BSA). These data indicate that the interaction of Rad52 with RPA increases the affinity of RPA for ssDNA significantly, in a Rad52 concentration-dependent manner.

In the GMSA, the affinities of the RPA:Rad52 and RPA:Rad52(218–418) complexes were all high enough to be near or at stoichiometric binding conditions (the apparent  $K_A$  determined was close to the concentration of DNA used,  $13 \times 10^{-9} \text{ M}$ ). Under stoichiometric binding conditions, the apparent affinity constant represents a minimum affinity of the complex. Therefore, the stimulatory effect of Rad52 was studied using surface plasmon resonance (SPR) under high-salt conditions in order to obtain equilibrium binding conditions (Table 1, rows 5–10). Raising the salt concentration to 1 M lowered the affinity of RPA for ssDNA by 3.6-fold ( $K_A = 3.9 \times 10^8 \text{ M}^{-1}$ ). Even under high-salt conditions, the binding of Rad52(218–418) was stimulatory and raised the affinity of RPA threefold to  $12 \times 10^8 \text{ M}^{-1}$  (Table 1, row 6).

The effect of salt on the RPA:Rad52 complex was then explored through a modified ELISA assay (Figure 7). It was found that salt concentrations higher than 250 mM KCl reduced the wild-type RPA:Rad52 complex by more than 50% under the conditions of the ELISA. At 1 M salt, ~5% of the complex remained (Figure 7(a)). This is not surprising, since the interaction is thought to be mediated partly by electrostatics through an acidic patch on RPA32CTD and a basic patch on Rad52.<sup>10</sup> The

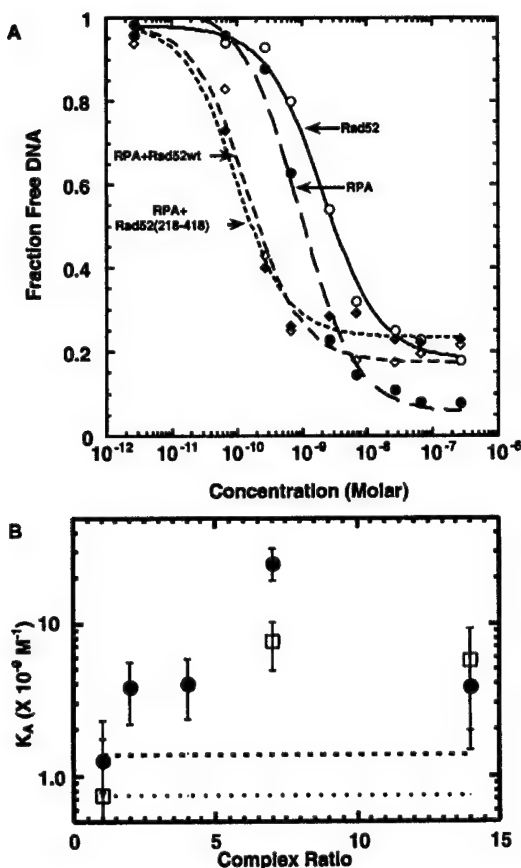


**Figure 6.** ssDNA binding data for RPA, Rad52 and RPA:Rad52 complexes. (a) Representative ssDNA binding isotherms obtained from GMSA as described in Materials and Methods for RPA (filled circles, long-dash broken line; fitted binding constant  $K_a = 1.1 \times 10^9 M^{-1}$ ), Rad52 (open circles, continuous line;  $K_a = 0.75 \times 10^9 M^{-1}$ ), RPA:Rad52 (1:7 ratio) complex (open diamonds, short-dash broken line;  $K_a = 7.9 \times 10^9 M^{-1}$ ) and RPA:Rad52(218–418) (1:7 ratio) complex (filled diamonds, dotted line;  $K_a = 1.3 \times 10^{10} M^{-1}$ ). Lines are the best fit curves obtained by non-linear least-squares fitting. (b) Binding affinity for ssDNA for RPA, Rad52 and RPA:Rad52 complexes. The measured association constants were measured by GMSA and plotted against the molar ratio of Rad52 monomer to RPA heterotrimer. The broken line indicates the affinity of wild-type RPA heterotrimer and the dotted line indicates the affinity of wild-type Rad52. The affinity of RPA:Rad52 complexes at various ratios of Rad52 to RPA are plotted with open squares for wild-type Rad52, and filled circles for Rad52(218–418). The plotted  $K_a$  ( $\times 10^9 M^{-1}$ ) values were 0.74 (0.24, V), 0.75 (0.15, F), 7.5 (2.6, S), and 5.6 (3.7, F) for wild-type Rad52 at ratios of 0:1, 1:1, 1:7 and 1:14 to RPA, respectively. For Rad52(218–418) the values were 1.3 (0.5, V), 3.8 (1.6, F), 4.1 (1.7, F), 25 (6.1, S), and 3.9 (2.4, F) at ratios of 1:1, 1:2, 1:4, 1:7 and 1:14 to RPA, respectively.

RPA:Rad52(218–418) complex was studied by SPR and it was slightly more resistant to salt than wild-type, needing more than 400 mM salt to reduce the complex by 50% (Figure 7(c)). At 1 M salt, ~15% of the RPA:Rad52(218–418) complex remained. Results for RPA14/32:Rad52 were similar (Figure 7(b)). The RPA70 $\Delta$ C442:Rad52(218–418) complex also showed sensitivity to salt and required more than 300 mM salt to reduce the complex by half, and retained 30% of the complex at 1 M salt (Figure 7(d)). This indicates that the majority of the RPA70 interaction is mediated by electrostatic interactions but to a slightly lesser extent than RPA14/32 or the wild-type heterotrimer. It was concluded that even though the salt conditions of the SPR assay appear to be diminishing the protein–protein interaction between RPA and Rad52, the stimulation of RPA's affinity for ssDNA was still seen (Table 1).

In order to help deconvolute the contributions of RPA70 and RPA32 to the stimulation of ssDNA binding by Rad52(218–418), five mutant forms of RPA were studied (RPA32RKN, RPA32WF, RPA32 $\Delta$ C224, RPA32 $\Delta$ C241, and RPA14/32; Figure 2). For the RPA32RKN mutant, conserved polar residues, homologous to those that interact with ssDNA in RPA70,<sup>22</sup> were replaced with alanine. The RPA32WF mutant has two conserved aromatic residues mutated to alanine. Disruption of the corresponding aromatic residues in scRPA has been found to disrupt interactions with DNA of the mutated domain.<sup>23</sup> When binding to a 30 residue oligonucleotide was examined, these mutants have the same affinity as wild-type for ssDNA (Figure 2). This is consistent with previous studies showing that the central domain of RPA70 is primarily responsible for binding to short oligonucleotides.<sup>19</sup> The RPA32RKN and RPA32WF forms of RPA also showed the same affinity for Rad52 as wild-type RPA (Figure 3(d)) but were not stimulated to bind ssDNA by Rad52(218–418) (Table 1, rows 7 and 8). Mutants with the CTD of RPA32 deleted, RPA32 $\Delta$ C224 and RPA32 $\Delta$ C241, have diminished binding for Rad52 (Figure 3(d)) and were not stimulated by Rad52(218–418) (Table 1, rows 9 and 10). No binding to ssDNA was detected for the RPA14/32 heterodimer alone or for the RPA14/32:Rad52 complex (Table 1, row 4), indicating that the presence of RPA70 in the RPA complex is required for stimulation. These results show that the increase in DNA affinity of the RPA:Rad52 complex is mediated through DNA binding by RPA32. They suggest that Rad52 binding to both RPA32 and RPA70 is required for stimulation.

#### RPA binding to Rad52 displaces higher-level self-association of Rad52

Human Rad52 forms large aggregates in solution. Two regions of Rad52 are responsible for aggregate formation (Figure 1). The self-association domain in the N-terminal half of Rad52 is



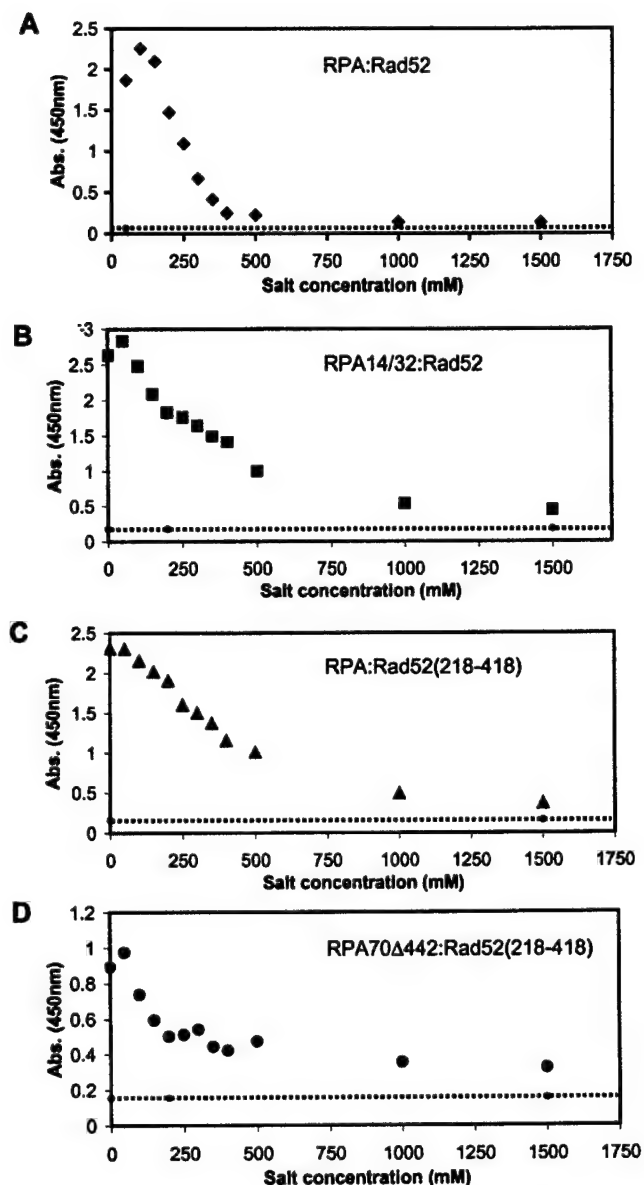


**Figure 7.** The effect of ionic strength on the RPA:Rad52 complex. A modified ELISA assay using the OPD substrate was used to study the effect of increasing ionic strength on the (a) wild-type RPA:Rad52 complex, (b) RPA14/32:Rad52 complex, (c) RPA:Rad52(218-418) complex, and (d) RPA70Δ442:Rad52(218-418). The dotted line indicates the baseline as determined with BSA. Antibody to RPA70 was used (Calbiochem) to detect wild-type RPA and RPA70ΔC442, and antibody to RPA32 was used to detect RPA14/32.

responsible for heptameric ring-formation and elements in the C-terminal half of the protein participate in the formation of higher-order complexes of rings.<sup>14</sup> The Rad52(218-418) mutant contains the C-terminal elements for the higher-order self-association and does not form rings. Rad52(218-418) contains the binding surface for RPA (Figure 1). The average molecular mass ( $M$ ) of the proteins and complexes in solution were measured by static light-scattering (SLS) and the ability of Rad52(218-418) to self-associate into higher-ordered complexes in the presence of RPA14/32 and RPA heterotrimer was tested (Table 2 and Figure 8).

Individual proteins were characterized by SLS first. Due to the higher-order self-association of Rad52, the  $M$  value of the wild-type protein is very sensitive to concentration and is not suitable for SLS. The  $M$  value for Rad52(218-418) is also concentration-dependent, but less so than wild-type and a narrow concentration range could be studied. A consistent size at low concentrations between 0.2 and 1.2 mg/ml was  $102(\pm 25)$  kDa and corresponded to a trimeric Rad52(218-418) complex (Table 2, row 1). Higher concentrations result in a shift in the  $M$  value to  $153(\pm 40)$  kDa equivalent to a tetrameric complex of Rad52(218-418) as was shown previously.<sup>14</sup> The RPA14/32

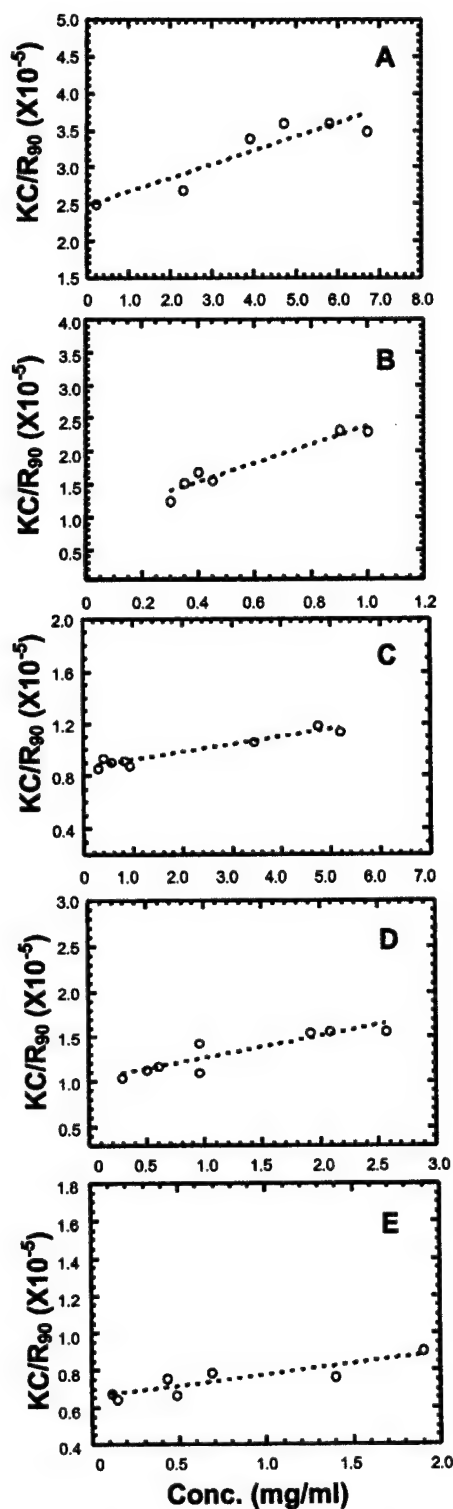


Figure 8. Static light-scattering data used for the molecular mass determinations summarized in Table 2. (a) RPA14/32, (b) Rad52(218-418), (c) RPA, (d)

heterodimer alone had an  $M$  value of  $42(\pm 11)$  kDa, which corresponds to a single heterodimer in solution (Table 2, row 3). Previous studies at three-fold higher protein concentrations indicated a dimer of dimers in solution.<sup>14</sup> SLS measurements of RPA heterotrimer alone show an  $M$  value of  $117(\pm 11)$  kDa (Table 2, row 2), which is consistent with previous results with the RPA heterotrimer obtained by hydrodynamic analysis and analytical ultracentrifugation.<sup>21,43</sup> These data indicate that these preparations of RPA14/32 and RPA heterotrimer have equal molar ratios of RPA14, RPA32 and RPA70 subunits.

Complex formation between RPA and Rad52 appears to disrupt the trimeric aggregates of Rad52(218-418). When Rad52(218-418) was added to RPA14/32 and RPA heterotrimer in an equal molar ratio of monomer to heterodimer or heterotrimer, the resulting complexes had  $M$  values of  $99(\pm 22)$  kDa and  $152(\pm 28)$  kDa, respectively (Table 2, rows 4 and 5). The RPA14/32:Rad52(218-418) and RPA:Rad52(218-418) complexes show an increase in molecular mass of approximately one Rad52(218-418) subunit. There was no increase in the polydispersity, as indicated by the standard deviation of the  $R_{90}$ , upon complex formation. This indicates that aggregates of Rad52(218-418) or free RPA were not detected. These data indicate that the binding of RPA to Rad52(218-418) is very effective at disrupting the higher-order self-association of Rad52.

## Discussion

### Regions of RPA important for binding Rad52

Two interaction sites on RPA for Rad52 were defined by the ELISA studies on a large number of RPA mutants to include RPA70 residues 168-326 and RPA32 residues 224-270 (Figure 9). Previous work had identified a specific interaction between human Rad52 and RPA and implicated the acidic CTD of RPA32 as the primary binding region for Rad52.<sup>10</sup> The possibility of an interaction between RPA70 and Rad52 had been eliminated because two RPA70 mutants (called p70d293-373 and p70d374-458) studied retained the ability to bind Rad52. Apparently, these deletions did not disrupt the RPA70:Rad52 binding site, which has been found in this work to be located between residues 169 and 382. The relative affinities of the RPA32 and RPA70 sites for Rad52 remain to be determined.

The two interaction sites on RPA for Rad52 are shared by Rad51 and XPA (Figure 9). When the RPA:Rad51 complex was studied by

Rad52(218-418):RPA14/32, (e) Rad52(218-418):RPA. Linear least-squares fitting was performed in Kaleidagraph and the correlation coefficients are 0.82, 0.92, 0.98, 0.96, and 0.89 for (a)-(e), respectively.



Table 2. Static light scattering data for forms of RPA, Rad52 and RPA:Rad52 complexes

Sample <sup>a</sup>	Conc. range (mg/ml)	R <sub>H</sub> <sup>b</sup> (nm)	C <sub>p</sub> /R <sub>H</sub> <sup>c</sup>	SLS M (kDa)	Error <sup>d</sup> (kDa)	Predicted M (kDa)	Complex <sup>e</sup> size
1. Rad52(218–418) <sup>f</sup>	0.2–1.2	4.71 (1.54)	0.321	102	25	38	2.7
2. RPA	0.1–5.0	5.17 (1.10)	0.203	117	11	110	1.1
3. RPA14/32	0.2–4.0	3.78 (0.93)	0.246	42	11	44	0.96
4. RPA14/32:Rad52(218–418)	0.2–3.0	4.41 (1.34)	0.364	99	22	82	1.2
5. RPA:Rad52(218–418)	0.1–4.0	5.21 (0.98)	0.193	153	28	148	1.0

<sup>a</sup> Samples were mixed on a one RPA heterodimer or heterotrimer to one Rad52 monomer ratio.

<sup>b</sup> Average R<sub>H</sub> with standard deviation in parentheses is reported from DynaLS.

<sup>c</sup> The average value of the polydispersity divided by the hydrodynamic radius.

<sup>d</sup> Derived from the reciprocal of the y intercept error (See Figure 8).

<sup>e</sup> Complex size is experimentally determined molecular mass divided by the predicted molecular mass.

<sup>f</sup> The size of Rad52(218–418) has been measured by several methods, including scanning transmission electron microscopy, gel-permeation chromatography and DLS, and ranged from three to four subunits depending on the protein concentration.<sup>14</sup> Due to the propensity of Rad52 to form higher-order complexes, wild-type was excluded from SLS experiments and Rad52(218–418) was kept at low concentrations.

immunoprecipitation a subset of the same RPA mutants were used.<sup>37</sup> The 168–326 region on RPA70 was shown to be important for complex formation with Rad51. A role for RPA32 in the complex was not studied completely, but RPA14/32 was shown to coimmunoprecipitate with Rad51. These results appear to imply a role for RPA32 in binding Rad51 that deserves further study. The regions identified for binding XPA are similar to Rad52 but do not overlap exactly.<sup>41</sup> Also, the XPA interaction with RPA14/32 was substantially lower than heterotrimeric RPA.

It is intriguing that the RPA heterodimer binds as tightly to Rad52 as the RPA heterotrimer. At present, a full explanation of this activity cannot be given but there are two likely explanations for

this observation. The heterodimer may adopt a slightly different conformation when RPA70 is not present that promotes Rad52 binding. For example, the RPA32CTD could be more accessible in the absence of RPA70 and the binding of Rad52 promoted by ease of access to RPA32CTD. Alternatively, the CTDs of two RPA14/32, in a

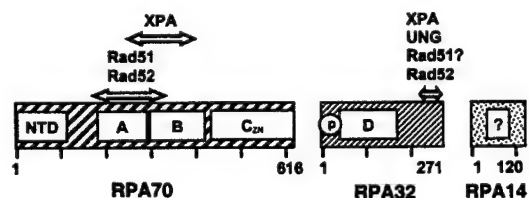


Figure 9. Comparison of binding of Rad52, Rad51, XPA and UNG to RPA. Real and putative DNA-binding domains (DBDs) are indicated in boxes as follows. On RPA70: DBD-A, includes residues 181–290; DBD-B, includes residues 300–422; DBD-C<sub>DN</sub>, includes residues 432–616 and contains a zinc finger; and DBD-NTD, includes residues 1–110. On RPA32: DBD-D, includes residues 43–171.<sup>19,22,23,26,35,47,54</sup> Another OB fold, indicated by a ?, exists on RPA14 that may or may not bind ssDNA.<sup>24</sup> The N terminus of RPA32, which becomes hyperphosphorylated during the cell-cycle and in response to DNA damage, is indicated by a p in a circle. The regions involved in binding Rad52 have been narrowed down to include RPA32 residues 224–271 and RPA70 residues 169–326; Rad51 to include RPA70 residues 169–326 and may possibly involve the C terminus of RPA32;<sup>37</sup> XPA to include RPA32 residues 224–271 and RPA70 residues 236–382;<sup>41</sup> and UNG binds to the RPA32CTD.<sup>35</sup> The regions on Rad52, XPA and UNG thought to bind RPA32CTD share limited homology.<sup>40</sup>

	uu u *u u
	bbb bbbb
RPA32 (252–267)	EGHIYS--TVDD-DHFKST
	EG   S VD       T
RPA70 (218–236)	EGKLFSLELVDESGEIRAT
	bbbbbbbbbbbb bbbbbbb
	s s sssss d d
<b>A</b>	
<i>H. sapiens</i>	EGKLFSLELVDESGEIRAT
<i>D. melanogaster</i>	EGKLFSMDLMDESGEIRAT
<i>S. cerevisiae</i>	DGKLFNVNFLDTSGEIRAT
<i>S. pombe</i>	EGKLFSVNLLDESGEIRAT
<i>X. laevis</i>	EGKLFSIEMVDESGEIRAT

Figure 10. Sequence analysis of the putative binding site for Rad52 on RPA70. (a) In line 1, a u indicates RPA32 residues shown to bind UNG peptide<sup>40</sup> and a \* indicates the position of the point mutation D228Y that disrupts Rad52-dependent double-strand break repair in *S. cerevisiae*.<sup>45</sup> In line 2, a b indicates RPA32 residues with  $\beta$ -strand secondary structure. Line 3, the sequence for residues 252–267 of RPA32. Line 4, identical homologous residues between RPA32 and RPA70 are indicated with the amino acid and similar residues are indicated with a vertical line. Lines 5 and 6, the sequence for residues 218–236 of RPA32 and the residues in  $\beta$ -strands are given.<sup>22</sup> Line 7, an s indicates surface-accessible residues and a d indicates residues interacting with ssDNA on RPA70. (b) Peptide sequences of RPA70 residues 218–236 from *Homo sapiens*, *S. cerevisiae*, *Schizosaccharomyces pombe*, *Drosophila melanogaster*, and *Xenopus laevis*. Amino acid residues that are identical with those of *H. sapiens* are in bold. Sequence alignments were performed using the Lipman–Pearson protein alignment available in Lasergene Navigator software (DNASTAR, Inc.) with the following settings: kTuple 2, gap penalty 4 and gap length penalty 6.

dimer-of-dimers, could closely approximate the surface of the RPA heterotrimer. There is evidence in the literature that RPA14/32 can assemble to form a dimer-of-dimers.<sup>24,44</sup> In this case, two RPA32 CTDs would be bound to Rad52, one in the normal RPA32 site of Rad52 and one in the Rad52 site normally occupied by RPA70. Evidence for the physiological relevance of the heterodimer in apoptosis makes the high affinity of it for Rad52 (and Rad51) even more intriguing.<sup>29,32</sup>

#### Putative Rad52 binding site on RPA70

We propose that the Rad52 interaction surface on RPA32 and RPA70 are similar in sequence composition. Two pieces of experimental evidence support this proposal. First, the ionic strength data (Figure 7) shows that both of the RPA14/32:Rad52 and RPA70Δ442:Rad52 complexes are disrupted by increasing concentration of salt, which indicates that both interaction surfaces involve electrostatic interactions, also supports this proposal. Secondly, the same region on Rad52 binds RPA14/32 and RPAΔ442 (Figure 5). To further explore this idea, a search for sequence homology was performed between RPA70(169–326) and RPA32(224–271). A homologous, acidic 19 residue peptide, including RPA70 residues 218–236 was found (Figure 10(a)). This putative Rad52 binding surface, RPA70(218–236), is 32% identical with and 79% similar in sequence to RPA32(252–267) and lies completely within DBD-A. This peptide contributes a small acidic patch to the surface of RPA70 and is neighbored by basic residues involved in binding ssDNA.

NMR and X-ray crystallographic structural information is available for the RPA32(252–267) and RPA70(218–236) peptides and is summarized on lines 1, 2, 6 and 7 of Figure 10(a).<sup>22,25,40</sup> The RPA32(252–267) peptide contains a binding surface for UNG2 and XPA, as well as Rad52.<sup>40</sup> In the NMR structure, the side-chains of residues 252, 253, 256, 261 and 267 are involved directly in binding the UNG peptide (line 1, Figure 9(a)) and are well conserved in the RPA70(218–236) peptide (Figure 10(b)). In the crystal structure of RPA70(181–422), the RPA70(218–236) peptide includes a tight turn between two antiparallel  $\beta$ -strands and is near residues involved in DNA binding (line 6, Figure 10(a)).<sup>22,25</sup> Notably, residues 218, 220, 228, 229, 230, and 232 are surface-accessible and are not involved in DNA binding (line 7, Figure 10(a)). DNA-binding residues are nearby and included in this sequence (residues 234 and 236) but their side-chains are mainly positioned on a different tight turn and on the opposite face of the  $\beta$ -sheet than the putative Rad52 binding surface. The 214–217 loop that moves upon DNA binding is just upstream from this sequence.<sup>25</sup> The sequence of the RPA70(218–236) peptide is well conserved (Figure 10(b)). Studies in yeast support the role of the RPA70(218–236) peptide in break repair. In *S. cerevisiae*, the mutation of Asp228 to

Tyr on scRPA70 altered Rad52-dependent DSB repair.<sup>45</sup> This mutation changes an acidic residue to a neutral residue, thereby lowering the electrostatic potential of the surface and possibly changing protein–protein interactions. In summary, the structural homology of the RPA32(252–267) and RPA70(218–236) peptides was not identical, but many secondary structure units are retained and the location on the surface of residues known to be important in protein–protein interactions are strictly conserved. Considering the available data, RPA70(218–236) is proposed to include the binding site for Rad52 on RPA70. Further experimentation will be needed to test this hypothesis.

#### The involvement of RPA32 in the enhanced ssDNA binding affinity of the RPA:Rad52 complex

The wild-type RPA:Rad52 complex has at least fivefold higher affinity for dT<sub>30</sub> than RPA alone. In these studies, DNA-binding to a short oligonucleotide 30 residues in length was analyzed. This length corresponds to the occluded binding site size of RPA.<sup>20</sup> Under these conditions, cooperative binding should not occur and only 1:1 RPA:DNA complexes should form. This means that in the RPA:Rad52 complex, Rad52 is probably not interacting with the DNA. This interpretation is supported by the finding that Rad52(218–418), which does not interact with ssDNA but interacts with RPA strongly, enhanced the equilibrium association constant by at least 18-fold. We conclude the effect of Rad52 binding must change the structure of RPA to facilitate higher ssDNA binding. The reason enhancement of Rad52(218–418) is higher than wild-type Rad52 is not known and could be because the ring-forming region of this mutant is missing. Mutations of residues in the OB-fold of RPA32 obliterate this stimulation and thereby support a role for RPA32 in the enhanced binding of ssDNA. Deletion of the RPA32 C-terminal interaction domain for Rad52 also disrupts the increase in affinity. These data indicate that the interaction between RPA and Rad52 is needed to increase the affinity through RPA32. To our knowledge, this is the first example of complex formation increasing the affinity of RPA through the RPA32 subunit. Similar enhancement of RPA ssDNA binding affinity has been seen with the DNA-binding proteins SV40 T-antigen and Gal4/VP16 (K. A. Braun, Y. Lao & M.S.W., unpublished results).<sup>46</sup>

These experiments do not address the effects of Rad52 on cooperative binding of RPA or of binding to long ssDNA lattices. Additional studies will be necessary to determine whether Rad52 stimulates RPA binding under cooperative binding conditions.

Data from a mutational analysis of the relative contribution of the four DNA-binding domains of *S. cerevisiae* RPA to ssDNA-binding affinity

supports the role of RPA32 in binding ssDNA. It showed that DBD-A (in scRPA70) played a primary role in binding short oligonucleotides of 12 nt or less and DBD-D (in scRPA32) interacts with longer oligonucleotides of 27 nt or more.<sup>23</sup> A sequential model of binding was proposed in which DBD-A is responsible for the initial interaction with ssDNA, that domains A, B and C (scRPA70) contact 12–23 nt of ssDNA and that DBD-D (scRPA32) is needed for substrates greater than 23 nt in length. It has been reported that the binding affinity of the RPA14/32 heterodimer is stimulated when the N and C termini of RPA32 were truncated.<sup>47</sup>

Contrary to our initial hypothesis, these data indicate that the stimulation of RPA ssDNA affinity by Rad52 is through ssDNA binding to the RPA32 subunit and not the major ssDNA-binding site in RPA70. This stimulation is mediated by Rad52 binding, is enhanced at higher concentrations of Rad52, and requires that RPA70 be present in the heterotrimer. There are two likely mechanisms to explain these observations. First, the binding of Rad52 to RPA32 may directly open the ssDNA-binding domain within RPA32 (Figure 9, DBD-D). Second, the binding of Rad52 may be affecting the global structure of the heterotrimer and stimulate RPA32 binding in an indirect manner.

#### Implications for DSB repair mechanism

Three pathways are known to repair double-strand breaks.<sup>1,48</sup> Their relative importance and function between the species is still under investigation. Homologous recombination is thought to be the predominant pathway in *S. cerevisiae*, and non-homologous end-joining as the dominant pathway in humans. Together, RPA and Rad52 can also perform single-strand annealing to repair DSBs in DNA containing repetitive sequences. Homologous recombination has been reconstituted *in vitro* for human and *S. cerevisiae* proteins.<sup>7,8,39</sup> In yeast, the binding of scRad52 is thought to facilitate scRad51 filament formation by displacing scRPA during homologous recombination.<sup>5</sup> The enhanced affinity of the RPA:Rad52 complex for ssDNA indicates that the mechanism of homologous recombination in humans may be different from that in *S. cerevisiae* and it is unlikely that the binding of human Rad52 displaces RPA from ssDNA. On the other hand, the stimulation of RPA ssDNA binding by Rad52 may partly explain the enhanced single-strand annealing seen when RPA is combined with Rad52.<sup>4,6,49</sup> A full understanding of the interplay between ssDNA, RPA, Rad52 and Rad51 binding awaits further experimentation on both human and yeast proteins, including the understanding of the effect protein–protein interactions have on ssDNA binding constants.

Due to the similarities of UNG, XPA and Rad52 in binding RPA, a “hand-off” model has been put forward for the assembly and coordination of different components of the DNA repair

machinery.<sup>40</sup> This model suggests that the dynamic assembly of the DNA repair machinery might be organized by multiple, competitive interactions with RPA. Our work contributes three pieces of data that support the hand-off model. First, the binding of Rad52 includes surfaces on both RPA32 and RPA70. Second, similar surfaces on RPA are employed for binding Rad52 and Rad51, that do not overlap completely in surface or activity with XPA (Figure 9). And third, the same surface on Rad52 that binds RPA is involved in the higher-order self-association of Rad52 rings. There is evidence that the higher-order complexes formed by Rad52 are important to its various functions in DSB repair. Rad52 interacts with itself to form heptameric ring complexes and higher-order interactions between ring complexes.<sup>9,12,14</sup> Human Rad52 was shown specifically to bind to DNA ends as an aggregated complex of rings.<sup>12</sup> Rad52 was also shown to facilitate the joining of DNA ends by bacteriophage T4 DNA ligase by Rad52–Rad52 intermolecular interactions.<sup>12</sup> The contribution of the higher-order self-association of Rad52 rings to single-strand annealing of complementary ssDNA ends has been confirmed by EM.<sup>15</sup> Here, we show that these Rad52 intermolecular interactions are disrupted in the presence of RPA, and thus RPA is competing for the same or nearby site on the C terminus of Rad52. The competition between RPA and Rad52 for the Rad52 C-terminal self-association surface may be of importance for the orchestration of the three DSB repair pathways. It was noted that high concentrations of human Rad52 were inhibitory to Rad51-mediated strand-exchange activity.<sup>8,37</sup> It is tempting to speculate that this inhibition was relieved by addition of RPA, perhaps through the displacement of higher-ordered Rad52 ring complexes by RPA binding. In conclusion, dynamic protein–protein and protein–DNA interactions involving complexes of RPA, Rad52 and Rad51 appear to be important component of DSB repair.

## Materials and Methods

### Generation of Rad52 monoclonal antibodies

Initial injections of 50 µg of wild-type Rad52 in complete Freund's adjuvant were given subcutaneously to eight to nine week old female Balb/C mice. Three additional boosts with 50 µg of antigen were given intraperitoneally without adjuvant at two week intervals. After the final injection, the mice were boosted two additional days and sacrificed by cervical dislocation on the fourth day. Splenocytes were isolated by passage through a wire mesh and red blood cells were removed by incubation with red blood cell lysis buffer (Sigma) on ice for ten minutes. Primary splenocytes were fused with the mouse myeloma cell line P3/NS1/1-Ag4-1 (American Type Culture Collection (ATCC), Rockville, MD.) in the presence of PEG (1300–1600 Da). The complete fusion was plated in 96-well plates and medium containing aminopterin was added the following day to eliminate unfused myeloma cells. Hybridoma

supernatants were screened by Western blot of bacterially expressed Rad52. Positive hybridomas were cloned by limiting dilution to isolate a clonal population of antibody-producing cells. Hybridomas were maintained in HY medium (Sigma) supplemented with 20% (v/v) fetal bovine serum (Hyclone Laboratories, Logan, UT). In total, 64 hybridomas cell lines were isolated. The epitopes of the secreted antibodies were mapped coarsely to the domains of Rad52 by Western blot with wild-type Rad52, Rad52(1–192), Rad52(1–303) and hRad52(1–340). Six antibodies that recognized different domains of Rad52 were identified and used in ELISA and immunoprecipitation.

#### Generation of Rad52 deletion mutant constructs

Wild-type human Rad52 (pRad52wt), Rad52(1–192), Rad52(1–303), and Rad52(1–340) pET28 expression plasmids, each with six histidine residues on the C terminus, were a gift from Dr M. Park (Los Alamos National Laboratories). Rad52(218–418) was prepared by amplifying the specific coding region of the wild-type gene in pRad52wt. The N-terminal PCR primer was: 5'-CAGCTGCAGCAGGTGACCTCCCTTCC-3' and the C-terminal PCR primer was 5'-GTGG-CCTGgaatTCAGTtAGATGGAT-3', which contained an engineered unique downstream *Eco*RI restriction site after the stop codon (underlined). PCR was performed using Taq polymerase (Promega) in a DNA thermal cycler (Perkin Elmer) using standard conditions. The PCR product was cloned into a pBAD/Thio-TOPO fusion vector (INVITROGEN) by TA-TOPO cloning. This ligation creates a fused thioredoxin gene N-terminal to the Rad52(218–418) gene sequence. The fusion protein gene sequence was then amplified from the pBAD/Thio-TOPO fusion vector using oligonucleotides: upstream 5'-CCGACCGcAtATGGCCCTGGGACACC-3' and the same downstream primer. The upstream primer contained the upstream thioredoxin start sequence and an engineered *Nde*I site. The sequence was ligated into the *Nde*I site and *Eco*RI site of a pET28 vector. The resulting fusion protein contained an N-terminal His<sub>6</sub> tag preceding a thioredoxin tag sequence and the Rad52(218–418) gene sequence.

#### Protein purification

Wild-type and mutant Rad52 were expressed and purified under reducing conditions as described.<sup>14</sup> The Rad52(218–418) purification was modified to include dialysis into 50 mM Caps (pH 10.2), 1 M KCl, 2% (v/v) glycerol, 0.5 mM *n*-hexyl-glucoside, 1 mM DTT, 1 mM EDTA and then loaded onto a Superdex 200 gel-filtration column. The eluted protein was stored in this buffer. Wild-type and mutant RPA were purified as described.<sup>19,44,50,51</sup> Protein concentrations were determined by the Bradford method using BSA as a standard. The concentrations of RPA, RPA 14/32, and Rad52(218–418) were corrected using extinction coefficients of  $8.44 \times 10^4$ ,  $2.34 \times 10^4$  and  $3.41 \times 10^4$  at 280 nm from precipitated protein denatured with GuHCl. For Rad52(218–418) practically identical concentrations were given by both methods. For RPA,  $A_{280}$  gave 1.2-fold lower concentrations.

Protein complexes were formed for static and dynamic light-scattering by adding equal molar amounts of RPA or RPA14/32 with Rad52(218–418) in a 15 ml micro-concentrator (Centricon-50). The protein solutions were

diluted  $\geq 20$ -fold in Rad52/RPA binding buffer (50 mM Hepes (pH 7.8), 150 mM KCl, 2% glycerol, 0.5 mM *n*-hexylglucoside, 1 mM DTT, 1 mM EDTA). Then the proteins were concentrated at 4 °C for 8–12 hours at 500 g and to allow complexes to form.

#### Enzyme-linked immunosorbent assay (ELISA)

The ELISA was performed as described.<sup>14,35</sup> The substrates used were (2',2'-azinobis[3-ethylbenzothiazoline-6-sulfonic acid] (ABTS), 3,3',5,5' tetramethyl benzidine(TMP) or *o*-phenylenediamine (OPD) in phosphate buffer and 0.01% (v/v) hydrogen peroxide. For ABTS, the absorbance was monitored at 405 nm. For TMP and OPD, the absorbance at 450 nm was monitored.

In order to study the effect of salt on the RPA:Rad52 complexes, a slightly modified ELISA protocol was used where the second protein (RPA) was diluted with a range of different concentrations of salt before it was allowed to interact with Rad52. This interaction step was followed by a wash step before detection of bound RPA with antibody.

#### Immunoprecipitation

Purified RPA (10 pmol of either wild-type RPA or RPA32A224) was mixed with 20 pmol of Rad52 in a 6  $\mu$ l reaction volume containing HM buffer (30 mM Hepes (pH 7.8), 0.5% (w/v) inositol, 0.01% (v/v) NP40, 1 mM DTT, 5 mM MgCl<sub>2</sub>) at room temperature for one hour. Each reaction was immunoprecipitated with 300  $\mu$ l of anti-Rad52 hybridoma conditioned supernatant and rocked at 4 °C for 30 minutes. Then 50  $\mu$ g of anti-mouse affinity gel (ICN) was added to the antibody-antigen complex and the reaction rocked at 4 °C for 30 minutes. The beads were spun down and washed five times with TBST buffer (10 mM Tris-HCl (pH 8.0), 150 mM NaCl, 0.05% (v/v) Tween-20). Samples were separated by SDS-PAGE (8% polyacrylamide gel) and transferred to nitrocellulose. The nitrocellulose was cut horizontally at approximately 60 kDa. The top half was immunoblotted using a monoclonal antibody to RPA70 (Calbiochem). The bottom half was probed for histidine-tagged Rad52 with INDIA probe (Pierce) and visualized by chemiluminescence. Initial characterization by Western analysis using wild-type and mutant Rad52 allowed rough mapping of their epitopes: mAb1 and mAb2 mapped to residues 1–192, mAb3 to residues 193–303, mAb4 to residues 304–340, and mAb5 and mAb6 to residues 341–418 (Figure 1). To further characterize the Rad52 antibodies, the ability of any of the antibodies to disrupt the RPA:Rad52 interaction was explored by immunoprecipitation. In immunoprecipitation reactions, all six anti-Rad52 antibodies pull down the RPA:Rad52 complex and RPA32A224 complex equivalently.

#### Gel mobility-shift assay (GMSA)

Gel mobility-shift assays were performed as described but with slight modifications.<sup>18,21</sup> Binding assays were carried out in 15  $\mu$ l volume in FBB buffer (30 mM Hepes (diluted from 1 M stock at pH 7.8), 100 mM NaCl, 5 mM MgCl<sub>2</sub>, 0.5% inositol, 1 mM DTT). The indicated amount of protein(s) was then incubated with 2 fmol of radio-labeled dT<sub>30</sub> and 50  $\mu$ g/ml of BSA at 25 °C for 20 minutes. When protein mixtures were used, the proteins were premixed and incubated on ice for ten minutes prior to being added to the reaction mixtures. Reactions



were then brought to a final concentration of 4% glycerol, 0.01% (w/v) bromophenol blue and electrophoresed on a 1% (w/v) agarose gel in  $0.1 \times$  TAE buffer. The gels were then dried on DE81 paper and radioactive bands were visualized by autoradiography. The radioactivity in each band was quantified using a Packard Instant Imager. Binding isotherms were obtained by plotting the fraction of oligonucleotide remaining unbound *versus* RPA concentration. Intrinsic binding constants were determined by non-linear least-squares fitting the data to the Langmuir binding equation (KaleidaGraph-Synergy Software) as described.<sup>16,21</sup>

### Surface plasmon resonance (SPR)

Interaction of RPA, Rad52 or mutants with ssDNA was monitored using a surface plasmon resonance (SPR) biosensor instrument, Biacore 3000 (Biacore). The 5'-biotinylated dT30 DNA was diluted to 64 nM in a buffer containing 10 mM sodium acetate (pH 4.8), 1 M NaCl, 2 mM MgCl<sub>2</sub>, 0.005% (w/v) polysorbate-20, 1 mM DTT. Protein was injected into the ssDNA surface (30RU) using the kinject function of Biacore. Association phase was allowed for 600 seconds followed by 400 seconds of buffer injection period for dissociation. Following RPA and Rad52 binding, regeneration was performed with a quick injection of 100 mM NaOH. Data were analyzed using a simple Langmuir 1:1 model.

### Static and dynamic light-scattering

Dynamic light-scattering (DLS) was carried out using a DynaPro-801 molecular sizing instrument equipped with a micro-sampler (Protein Solutions). The instrument has a laser wavelength of 828.7 nm and a fixed scattering angle of 90°. DLS is based on the collected autocorrelation function of the scattered intensity. The acquisition time for all experiments was ten seconds. A 50 µl sample was passed through the filtering assembly into a 12 µl chamber quartz cuvette. All proteins were filtered with 20 nm filters (Whatman). The data were analyzed first with the Dynamics 4.0 software and then the DynaLS software. These gave consistent values for the hydrodynamic radius ( $R_H$ ) and polydispersity ( $C_p$ ). All distributions were monomodal, meaning a single distribution of molecules, for this study as defined by the baseline values range from 0.997–1.002. The sum of squares (SOS) error represents the error in the decay of the autocorrelation function. Good SOS errors are 5% or less. The resolution slider values were optimized by the DynaLS software. The resolution slider value represents the maximum allowable information about the distribution without including effects of noise.

Each of the static light-scattering (SLS) data points, at various concentrations, represents a single DLS experiment. The average intensity for approximately 25–30 data points (30–45 minutes) at a 90° angle was measured. This average intensity for each protein concentration was used to calculate Rayleigh ratios with toluene as the reference solvent. The SLS by a protein depends on the concentration, the scattered light

intensity, and the molecular mass as follows:<sup>52</sup>

$$\frac{KC}{R_{90}} = \frac{1}{M} + 2B_{22}C$$

where  $C$  is the protein concentration,  $R_{90}$  is the Rayleigh ratio at 90°,  $B_{22}$  is the second virial coefficient,  $M$  is the average molecular mass of the protein in solution, and  $K$  is the optical constant. Since the particles under study are more than ten times smaller than the wavelength, the shape of the particles does not need to be considered.

$$K = \frac{1}{N_A} \left( \frac{2\pi n_0}{\lambda^2} \right)^2 \left( \frac{dn}{dC} \right)^2$$

where  $N_A$  is Avogadro's number,  $\lambda$  is the wavelength,  $n_0$  is the refractive index of the solution and  $dn/dC$  is the refractive index increment of the protein solution with protein concentration. The value for  $dn/dC$  used here was 0.186 ml/g. The Rayleigh ratio ( $KC/R_{90}$ ) is plotted *versus* protein concentration and fit by linear regression. The molecular mass was obtained from the  $y$  intercept. The error was estimated from the linear least-squares fit to the data (KaleidaGraph). Sources of errors include intensity fluctuations and protein concentration measurements. All data points for SLS were monomodal distributions with SOS errors near 5% or below. For every SLS experiment,  $R_H$  was monitored and the differences due to higher concentration or aggregation were less than 5% of  $R_H$ . It was not possible to perform SLS experiments on wild-type Rad52 because of its significant dependence on  $R_H$  with concentration.<sup>14</sup>

### Acknowledgments

We thank Ye Lao, Jeff Ohren, Wasantha Ranatunga and Andre Walther for providing purified proteins and technical assistance; D. Margaret Wheelock for antibody production; Dr Min Park for providing Rad52 expression vectors for wild-type Rad52, Rad52(1–192), Rad52(1–303) and Rad52(1–340); and Krishnamurthy Rajeswari for her initial work in developing the Rad52(218–418) construct. This work was supported by the U.S. Army Medical Research and Materiel Command under DAMD17-98-1-8251 (to G.E.O.B.), DAMD17-00-1-0467 (to D.J.) and the National Institutes of Health RO1-GM44721 (to K.D. and M.W.).

### References

- Shinohara, A. & Ogawa, T. (1995). Homologous recombination and the roles of double-strand breaks. *Trends Biochem. Sci.* **20**, 387–391.
- Sung, P. (1997). Function of yeast Rad52 protein as a mediator between replication protein A and the Rad51 recombinase. *J. Biol. Chem.* **272**, 28194–28197.
- Benson, F. E., Baumann, P. & West, S. C. (1998). Synergistic actions of Rad51 and Rad52 in recombination and DNA repair. *Nature*, **391**, 401–404.
- Shinohara, A., Shinohara, M., Ohta, T., Matsuda, S. & Ogawa, T. (1998). Rad52 forms ring structures and cooperates with RPA in single-strand DNA annealing. *Genes Cells*, **3**, 145–156.
- New, J. H., Sugiyama, T., Zaitseva, E. & Kowalczykowski, S. C. (1998). Rad52 protein stimulates DNA strand exchange by Rad51 and replication protein A. *Nature*, **391**, 407–410.

6. Sugiyama, T., New, J. H. & Kowalczykowski, S. C. (1998). DNA annealing by RAD52 protein is stimulated by specific interaction with the complex of replication protein A and single-stranded DNA. *Proc. Natl Acad. Sci. USA*, **95**, 6049–6054.
7. McIlwraith, M. J., Dyck, E. V., Masson, J.-Y., Stasiak, A. Z., Stasiak, A. & West, S. C. (2000). Reconstitution of the strand invasion step of double-strand break repair using human Rad51 Rad52 and RPA proteins. *J. Mol. Biol.* **304**, 151–164.
8. Baumann, P. & West, S. C. (1999). Heteroduplex formation by human Rad52 protein effects of DNA end-structure, hRPA and hRad52. *J. Mol. Biol.* **291**, 363–374.
9. Van Dyck, E., Hajibagheri, N. M. A., Stasiak, A. & West, S. C. (1998). Visualisation of human Rad52 protein and its complexes with hRad51 and DNA. *J. Mol. Biol.* **284**, 1027–1038.
10. Park, M. S., Ludwig, D. L., Stigger, E. & Lee, S. H. (1996). Physical interaction between human RAD52 and RPA is required for homologous recombination in mammalian cells. *J. Biol. Chem.* **271**, 18996–19000.
11. Kagawa, W., Kurumizaka, H., Ikawa, S., Yokoyama, S. & Shibata, T. (2001). Homologous pairing promoted by the human Rad52 protein. *J. Biol. Chem.* **276**, 35201–35208.
12. Van Dyck, E., Stasiak, A. Z., Stasiak, A. & West, S. C. (1999). Binding of double-strand breaks in DNA by human Rad52 protein. *Nature*, **398**, 728–731.
13. Stasiak, A. Z., Larquet, E., Stasiak, A., Muller, S., Engel, A., Dyck, E. V. *et al.* (2000). The human Rad52 protein exists as a heptameric ring. *Curr. Biol.* **10**, 337–340.
14. Ranatunga, W., Jackson, D., Lloyd, J. A., Forget, A. L., Knight, K. L. & Borgstahl, G. E. O. (2001). Human Rad52 exhibits two modes of self-association. *J. Biol. Chem.* **276**, 15876–15880.
15. Dyck, E. V., Stasiak, A. Z., Stasiak, A. & West, S. C. (2001). Visualization of recombination intermediates produced by RAD52-mediated single-strand annealing. *EMBO Rep.* **2**, 905–909.
16. Wold, M. S. (1997). RPA: a heterotrimeric single-stranded DNA-binding protein required for eukaryotic DNA metabolism. *Annu. Rev. Biochem.* **66**, 61–91.
17. Iftode, C., Daniely, Y. & Borowiec, J. A. (1999). Replication protein A (RPA): the eukaryotic SSB. *Crit. Rev. Biochem. Mol. Biol.* **34**, 141–180.
18. Kim, C., Snyder, R. O. & Wold, M. S. (1992). Binding properties of replication protein A from human and yeast cells. *Mol. Cell. Biol.* **12**, 3050–3059.
19. Gomes, X. V., Henriksen, L. A. & Wold, M. S. (1996). Proteolytic mapping of human replication protein A: evidence for multiple structural domains and a conformational change upon interaction with single-stranded DNA. *Biochemistry*, **35**, 5587–5594.
20. Gomes, X. V. & Wold, M. S. (1996). Functional domains of the 70-kilodalton subunit of human replication protein A. *Biochemistry*, **35**, 10558–10568.
21. Kim, C., Paulus, B. F. & Wold, M. S. (1994). Interactions of human replication protein A with oligonucleotides. *Biochemistry*, **33**, 14197–14206.
22. Bochkarev, A., Pfuetzner, R. A., Edwards, A. M. & Frappier, L. (1997). Crystal structure of the DNA binding domain of replication protein A bound to DNA. *Nature*, **385**, 176–181.
23. Bastin-Shanower, S. A. & Brill, S. J. (2001). Functional analysis of the four DNA binding domains of replication protein A: the role of RPA2 in ssDNA binding. *J. Biol. Chem.* **276**, 36446–36453.
24. Bochkarev, A., Bochkareva, E., Frappier, L. & Edwards, A. M. (1999). The crystal structure of the complex of replication protein A subunits RPA32 and RPA14 reveals a mechanism for single-stranded DNA binding. *EMBO J.* **18**, 4498–4504.
25. Bochkareva, E., Belegu, V., Korolev, S. & Bochkarev, A. (2001). Structure of the major single-stranded DNA-binding domain of replication protein A suggests a dynamic mechanism for DNA binding. *EMBO J.* **20**, 612–618.
26. Jacobs, D. M., Lipton, A. S., Isern, N. G., Daughdrill, G. W., Lowry, D. F., Gomes, X. & Wold, M. S. (1999). Human replication protein A: global fold of the N-terminal RPA-70 domain reveals a basic cleft and flexible C-terminal linker. *J. Biomol. NMR*, **14**, 321–331.
27. Blackwell, L., Borowiec, J. & Mastrangelo, I. (1996). Single-stranded DNA binding alters human replication protein A structure and facilitates interaction with DNA-dependent protein kinase. *Mol. Cell. Biol.* **16**, 4798–4807.
28. Din, S.-U., Brill, S. J., Fairman, M. P. & Stillman, B. (1990). Cell cycle regulated phosphorylation of DNA replication factor A from human and yeast cells. *Genes Dev.* **4**, 968–977.
29. Treuner, K., Okuyama, A., Knippers, R. & Fackelmayer, F. O. (1999). Hyperphosphorylation of replication protein A middle subunit (RPA32) in apoptosis. *Nucl. Acids Res.* **27**, 1499–1504.
30. Rodrigo, G., Roumagnac, S., Wold, M. S., Salles, B. & Calsou, P. (2000). DNA replication but not nucleotide excision repair is required for UVC-induced replication protein A phosphorylation in mammalian cells. *Mol. Cell. Biol.* **20**, 2696–2705.
31. Henriksen, L. A., Carter, T., Dutta, A. & Wold, M. S. (1996). Phosphorylation of human replication protein A by the DNA-dependent protein kinase is involved in the modulation of DNA replication. *Nucl. Acids Res.* **24**, 3107–3112.
32. Treuner, K., Findeisen, M., Strausfeld, U. & Knippers, R. (1999). Phosphorylation of replication protein A middle subunit (RPA32) leads to a disassembly of the RPA heterotrimer. *J. Biol. Chem.* **274**, 15556–15561.
33. Loo, Y.-M. & Melendy, T. (2000). The majority of human replication protein A remains complexed throughout the cell cycle. *Nucl. Acids Res.* **28**, 3354–3360.
34. Dimitrova, D. S. & Gilbert, D. M. (2000). Stability and nuclear distribution of mammalian replication protein A heterotrimeric complex. *Expt. Cell Res.* **254**, 321–327.
35. Braun, K. A., Lao, Y., He, Z., Ingles, C. J. & Wold, M. S. (1997). Role of protein–protein interactions in the function of replication protein A (RPA): RPA modulates the activity of DNA polymerase  $\alpha$  by multiple mechanisms. *Biochemistry*, **36**, 8443–8454.
36. Stigger, E., Drissi, R. & Lee, S. H. (1998). Functional analysis of human replication protein A in nucleotide excision repair. *J. Biol. Chem.* **273**, 9337–9343.
37. Golub, E. I., Gupta, R. C., Haaf, T., Wold, M. S. & Radding, C. M. (1998). Interaction of human RAD51 recombination protein with single-stranded DNA binding protein, RPA. *Nucl. Acids Res.* **26**, 5388–5393.
38. Hays, S. L., Firmenich, A. A., Massey, P., Banerjee, R. & Berg, P. (1998). Studies of the interaction between Rad52 protein and the yeast single-stranded DNA binding protein RPA. *Mol. Cell. Biol.* **18**, 4400–4406.
39. Song, B. W. & Sung, P. (2000). Functional interactions among yeast Rad51 recombinase, Rad52 mediator,

- and replication protein A in DNA strand exchange. *J. Biol. Chem.* **275**, 15895–15904.
40. Mer, G., Bochkarev, A., Gupta, R., Bochkareva, E., Frappier, L., Ingles, C. J. *et al.* (2000). Structural basis for the recognition of DNA repair proteins UNG2, XPA and Rad52 by replication factor RPA. *Cell*, **103**, 449–456.
  41. Walther, A. P., Gomes, X. V., Lao, Y., Lee, C. G. & Wold, M. S. (1999). Replication protein A interactions with DNA. I. Functions of the DNA-binding and zinc-finger domains of the 70-kDa subunit. *Biochemistry*, **38**, 3963–3973.
  42. Lao, Y. (2001). Multiple interactions between DNA and human replication protein A (RPA). PhD Dissertation, University of Iowa, Department of Biochemistry, Iowa City, IA.
  43. Sibenaller, Z. A., Sorensen, B. R. & Wold, M. S. (1998). The 32- and 14-kilodalton subunits of replication protein A are responsible for species-specific interactions with single-stranded DNA. *Biochemistry*, **37**, 12496–12506.
  44. Habel, J. E., Ohren, J. F. & Borgstahl, G. E. O. (2001). Dynamic light scattering analysis of full-length, human RPA14/32 dimer: purification, crystallization and self-association. *Acta Crystallog. sect. D*, **D57**, 254–259.
  45. Smith, J. & Rothstein, R. (1999). An allele of *RFA1* suppresses *RAD52*-dependent double-strand break repair in *Saccharomyces cerevisiae*. *Genetics*, **151**, 447–458.
  46. Lao, Y., Gomes, X. V., Ren, Y., Taylor, J. S. & Wold, M. S. (2000). Replication protein A interactions with DNA. III. Molecular basis of recognition of damaged DNA. *Biochemistry*, **39**, 850–859.
  47. Bochkareva, E., Frappier, L., Edwards, A. M. & Bochkarev, A. (1998). The RPA32 subunit of human replication protein A contains a single-stranded DNA-binding domain. *J. Biol. Chem.* **273**, 3932–3936.
  48. Haber, J. E. (1999). Gatekeepers of recombination. *Nature*, **398**, 665–667.
  49. Mortensen, U. H., Bendixen, C., Sunjevaric, I. & Rothstein, R. (1996). DNA strand annealing is promoted by the yeast Rad52 protein. *Proc. Natl Acad. Sci. USA*, **93**, 10729–10734.
  50. Henriksen, L. A., Umbricht, C. B. & Wold, M. S. (1994). Recombinant replication protein A: expression, complex formation and function characterization. *J. Biol. Chem.* **269**, 11121–11132.
  51. Gomes, X. V. & Wold, M. S. (1995). Structural analysis of human replication protein A; mapping functional domains of the 70-kDa subunit. *J. Biol. Chem.* **270**, 4534–4543.
  52. Kratochvil, P. (1987). *Classical Light Scattering from Polymer Solutions*, Elsevier, Amsterdam.
  53. Shen, Z., Peterson, S. R., Comeaux, J. C., Zastrow, D., Moyzis, R. K., Bradbury, E. M. & Chen, D. J. (1996). Self-association of human RAD52 protein. *Mutat. Res.* **364**, 81–89.
  54. Pfuetzner, R. A., Bochkarev, A., Edwards, A. M. & Frappier, L. (1997). Replication protein A: characterization and crystallization of the DNA binding domain. *J. Biol. Chem.* **272**, 430–434.
  55. Nagelhus, T. A., Haug, T., Singh, K., Keshav, K. F., Skorpen, F., Otterlei, M. *et al.* (1997). A Sequence in the N-terminal region of human uracil-DNA glycosylase with homology to XPA interacts with the C-terminal part of the 34-kDa subunit of replication protein A. *J. Biol. Chem.* **272**, 6561–6566.

Edited by J. O. Thomas

(Received 19 February 2002; received in revised form 13 May 2002; accepted 20 May 2002)